Biases in the Atlantic ITCZ in seasonal-interannual variations for a coarse and a high resolution coupled climate model

Takeshi Doi[1,2], Gabriel A. Vecchi[2], Anthony J. Rosati[2], and Thomas L. Delworth[2]

1 Atmospheric and Oceanic Sciences Program, Princeton University, Princeton, NJ, U.S.A.

2 NOAA/Geophysical Fluid Dynamics Laboratory, Princeton, NJ, U.S.A.

J. Climate

(in press, Mar. 30, 2011)

Corresponding author address: Takeshi Doi, Geophysical Fluid Dynamics Laboratory/NOAA, Princeton University Forrestal Campus, 201 Forrestal Road, Princeton, NJ 08542, USA

Tel: +1-609-452-6511

Email: Takeshi.Doi@noaa.gov

Abstract:

Using two fully coupled ocean-atmosphere models of CM2.1 (the Climate Model version 2.1 developed at the Geophysical Fluid Dynamics Laboratory) and CM2.5 (a new high-resolution climate model based on CM2.1), the characteristics and sources of SST and precipitation biases associated with the Atlantic ITCZ have been investigated.

CM2.5 has an improved simulation of the annual mean and the annual cycle of the rainfall over the Sahel and the northern South America, while CM2.1 shows excessive Sahel rainfall and lack of northern South America rainfall in boreal summer. This marked improvement in CM2.5 is due to not only high-resolved orography, but also a significant reduction of biases in the seasonal meridional migration of the ITCZ. In particular, the seasonal northward migration of the ITCZ in boreal summer is coupled to the seasonal variation of the SST and a subsurface doming of the thermocline in the northeastern tropical Atlantic, known as the Guinea Dome. Improvements in the ITCZ allow for better representation of the coupled processes that are important for an abrupt seasonally phase-locked decay of the interannual SST anomaly in the northern tropical Atlantic.

Nevertheless, the differences between CM2.5 and CM2.1 were not sufficient to reduce the warm SST biases in the eastern equatorial region and Angola-Benguela Area. The weak bias of southerly winds along the southwestern African coast associated with the excessive southward migration bias of the ITCZ may be a key to

improve the warm SST biases there.

1. Introduction

Climate conditions in the tropical Atlantic have to be simulated well in climate models for accurate prediction of the Atlantic Hurricane and drought (or flood) in the Sahel and South America (Emanuel 2005; Vecchi and Soden 2007; Hagos and Cook 2009). Also, the impacts of the Atlantic variations are not restricted to the Atlantic Basin and can have far-reaching effects (Dommenget et al. 2006; Zhang and Delworth 2006; Zhang et al. 2007; Sutton and Hodson 2005; Kucharski et al. 2011). However, many coupled GCMs suffer from serious biases in the tropical Atlantic (Davey et al. 2002). In particular, almost all CMIP3 (Coupled Model Intercomparison Project; Meehl et al. 2007) climate models for the Intergovernmental Panel on Climate Change Fourth Assessment Report (IPCC-AR4) show warm SST biases in the eastern equatorial Atlantic and produce a zonal SST gradient along the Atlantic equator with opposite sign to observations (Richter and Xie 2008). The warm SST bias in the eastern equatorial Atlantic still remains in the new generation of climate model, the Community Climate System Motel, version 4: CCSM4 (Grodsky et al. 2012; Muñoz et al. 2012). The lack of the cold tongue in the equatorial Atlantic will be one reason why many coupled GCMs fail to simulate and predict the Atlantic Niño (Stockdale et al. 2006), which is the most major climate mode in the tropical Atlantic (Zebiak 1993; Carton and Huang 1994). Richter and Xie (2008) showed that the origin of the biases is in the anomalously weak trade winds along the equator, which are associated with the ITCZ being displaced anomalously southward in boreal spring. Richter et al. (2011)

suggests the zonal surface wind errors along the equator were partially due to deficient precipitation over equatorial South America and excessive precipitation over equatorial Africa. Recently, the University Tokyo Coupled Model (Tozuka et al. 2006) was able to successfully simulate the zonal gradient of the annual mean SST (Doi et al. 2010). Interestingly, the model's ability to simulate this feature depends on deep convection scheme used (Tozuka et al. 2011).

In the tropical Atlantic climate, two types of air-sea coupled process are important: the zonal Bjerknes positive feedback (Bjerknes 1969) and the meridional Wind-Evaporation-SST (WES) positive feedback (Xie 1999). The Bjerknes feedback is associated with a zonal gradient of SST on the equator: 1) a weak zonal gradient of SST is responsible for weaker easterly wind on the equator, 2) weaker easterly winds deepen (shallow) thermocline, 3) warms (cools) SST in eastern (western) equatorial region. The outcome is the further weak easterly winds. The Bjerknes feedback develops the Atlantic Niño, which is characterized as a warm SST anomaly in the eastern equatorial Atlantic during boreal summer (Zebiak 1993; Carton and Huang 1994). The WES positive feedback is the interhemispheric two-way air-sea interaction between wind and SST, and is associated with meridional migrations of the ITCZ: 1) an anomalously northward migration of the ITCZ causes southwesterly (southeasterly) wind anomalies in the northern (southern) tropics leading to weaker trade winds, 2) this results in less (more) evaporation and thus suppressed (enhanced) latent heat loss from ocean, leading to warmer (colder) SST in the northern (southern) tropical Atlantic, 3) the outcome is the further northward migration of the ITCZ. The dominance of this

mechanism in the growth of the Atlantic Meridional Mode has been discussed in previous work (Carton et al. 1996; Chang et al. 1997; Xie 1999). The Atlantic Meridional Mode is characterized by the cross-equatorial meridional gradient of SST anomaly in the tropical Atlantic during boreal spring (Servain 1991; Xie and Carton 2004 for a recent review).

The Atlantic climate modes are closely linked with not only air-sea interactions between wind and SST, but also subsurface oceanic conditions. In the tropical Atlantic, two thermocline domes associated with ocean upwelling are found; the Angola Dome in the southeastern tropical Atlantic and the Guinea Dome in the northeastern tropical Atlantic (Mazeika 1967). Interannual variations of the Angola Dome in the South Atlantic are strongly influenced by the Atlantic Niño (Doi et al. 2007), while the interannual variations of the Guinea Dome are linked with the Atlantic Meridional Mode (Doi et al. 2009; 2010). In particular, Doi et al. (2010) pointed out that the Guinea Dome could play a critical role on the seasonal-phase locking of the interannual variations of the northern tropical Atlantic SST (Fig. 18 of Doi et al 2010). Although most studies on the Atlantic climate have focused on the atmospheric forcing or the sea surface field, considering the ocean dynamical roles of upwelling and stratification variations in climate models is important for understanding tropical Atlantic climate modes (Doi 2009) and hurricane intensity (Lloyd and Vecchi 2011).

In this paper, we investigate how tropical Atlantic biases are improved by comparing a fully coupled ocean-atmosphere climate model with a new high resolution climate model (including some changes to parameterizations, numerics and a land-

model). Our manuscript shows that many aspects of the simulation in the tropical Atlantic are significantly improved in the new model–yet others persists. The paper is organized as follows. In section 2, differences between coarse and high resolution coupled climate models and brief description of observational datasets are given. In section 3, the annual mean and the annual cycle of SST and rainfall in two models are explored. In the first half of section 3, we discuss the most severe biases in the eastern equatorial Atlantic**,** which still persist in the new high-resolution model. In the latter half, we focus on the meridional migration of the ITCZ in boreal summer and its coupled link with the SST and the Guinea Dome in the northern tropical Atlantic because the new model significantly improved the simulation of rainfall in the Sahel and South America. In section 4, we explore the interannual variation of the two models and observations with particular, focus on the seasonal phase-locking of the interannual variation in the northern tropical Atlantic SST. The final section is used for summary and discussions.

2. Models and observational datasets

a. GFDL-CM2.1

The detailed formulations of the Climate Model version 2.1 developed at the Geophysical Fluid Dynamics Laboratory (CM2.1) are described by Delworth et al. 2006, Gnanadesikan et al. 2006, Stouffer et al. 2006, and Wittenberg et al. 2006.

CM2.1 was part of the CMIP3 model comparison which contributed to the IPCC AR4, and CM2.1 has been shown to perform quite well for many global climate metrics (Knutson et al. 2006; Russell et al. 2006). CM2.1 is also the basis of experimental seasonal to decadal forecast systems in GFDL (Zhang et al. 2007). The oceanic component is based on the Modular Ocean Model version 4 (MOM4) code (Griffies et al. 2005). The horizontal resolution is 1° longitudinal and 1° latitudinal with enhanced tropical resolution (1/3° within 10° of the equator). There are 50 vertical levels and the vertical grid spacing is a constant 10m over the top 220m. Isopycnal mixing of tracers and layer thickness is based on the formulation by Gent and McWilliams (1990), Griffies et al. (1998), and Griffies (1998). The mixed-layer is represented by the K-profile parameterization (KPP) vertical mixing (Large et al. 1994). The shortwave penetration depends on prescribed spatio-temporally varying chlorophyll (Sweeney et al. 2005).

The atmospheric component is the AM2.1 atmosphere model (GFDL Global Atmospheric Model Development Team: GAMDT 2004), which consists of a finite volume dynamical core (Lin 2004) with 24 vertical levels, 2° latitude by 2.5° longitude grid spacing, K-profile planetary boundary layer scheme (Lock et al. 2000), and relaxed Arakawa-Schubert convection (Moorthi and Suarez 1992). The land model is LM2, which includes soil sensible and latent heat storage, groundwater storage, and stomatal resistance (GAMDT 2004). The coupled simulation is initialized from observed climatological oceanic condition at year 1 (Delworth et al. 2006) and then integrated subject to 1990 values of trace gases, insolation, aerosols, and land cover.

This radiative forcing yields a present-day control experiment. The atmosphere, ocean, land and sea ice exchange fluxes every two hours and no flux adjustments are employed. We have calculated monthly climatologies by averaging model monthly mean output for the 300 years. Then, we define anomaly fields as deviations from the monthly mean climatologies, after removing the decadal variability using an eight-year running mean filter.

b. GFDL-CM2.5

GFDL-CM2.5 is a new high-resolution model version that derives closely from GFDL-CM2.1 (Delworth et al. 2012). The oceanic component of CM2.5 uses a 0.25° horizontal resolution of MOM4p1 in the tropics with the z* vertical coordinate (Griffies 2010; Griffies et al. 2012), which varies from 28km near the tropics to 8km in polar regions. Its oceanic component is similar to that of the CM2.4 model used in Farneti et al. (2010). It is coupled to a 50km horizontal resolution atmosphere model with 32 vertical levels on a cubed-sphere grid (Lin 2004; Putman and Lin 2007). This formulation avoids the numerical problem arising from the convergence of meridians at the poles and allows grid boxes of roughly equal area over the globe. No flux adjustments are employed. The ocean model does not contain a parameterization for mesoscale eddy mixing. The advective scheme has been modified to yield substantially lower numerical diffusion, and a substantially smaller explicit viscosity than CM2.1 is employed. The land model is LM3 (Shevliakova et al. 2009; Milly et al. *in*

preparation), which represents snow and rain interception on vegetation, as well as water phase change in the soil and snow pack. CM2.5 is initialized and forced in similar fashion to CM2.1 (Delworth et al. 2012; Delworth et al. 2006); the oceanic initial condition is taken from the end of one-year spin-up from observed climatological conditions at rest and the atmospheric initial condition is taken from the end of a simulation with prescribed SSTs.

We used monthly mean output from a 280-year simulation of CM2.5 with 1990 radiative forcing. The monthly averaged climatology and interannual anomaly are calculated as the same manner in CM2.1. For reference, the atmospheric components of CM2.1 and CM2.5 forced by observed SST in 1981-2000 (AM2.1 and AM2.5) are also used.

c. Observational datasets

We use two SST datasets to evaluate the models: the Extended Reconstructed SST version 3 (ERSSTv3b; Smith et al. 2008) and, the Hadley Center SST (HadISST; Rayner et al. 2003). For wind stress and surface enthalpy fluxes, we used the NCEP/NCAR reanalysis data (Kalnay et al. 1996) and ECMWF 40-year reanalysis data (ERA40; Simmons and Gibson 2000). Also, surface enthalpy flux data from the objectively analyzed air-sea fluxes (OAFlux; Yu et al. 2006) are used. Monthly climatologies are calculated by averaging monthly observational data over 1960-2001, and then interannual anomalies are defined as deviations from the monthly mean

climatologies after subtracting the eight-year running mean values. Since the OAFlux project provides only latent and sensible heat fluxes in this epoch, the turbulent enthalpy fluxes of the OAFlux are combined with the radiative fluxes from the NCEP/NCAR reanalysis data (OAFlux-N), and with the ERA 40 reanalysis data (OAFlux-E). For precipitation data, Climate Prediction Center Merged Analysis of Precipitation dataset (CMAP; Xie and Arkin 1997) and Global Precipitation Climatology Project dataset (GPCP; Adler et al. 2003) are used for 1979-2001. The observed mixed-layer depth is estimated from the monthly climatology of the World Ocean Atlas 2005 data (WOA05; Locarnini et al. 2006), as the depth at which the potential density becomes larger than the surface density by 0.125 kg m^{-3}, as used by Levitus (1982).

3. Annual mean and annual cycle

We begin by exploring the annual mean fields of the tropical Atlantic SST in observations and the two climate models (Fig. 1). The SST near the northern South American coast is colder by about 1°C in CM2.1 than the observed SST of ERSSTv3. This bias is reduced in CM2.5, likely due to the more reasonable simulation of the North Brazil Current and the eddy activity in this area. Also, CM2.1 has a cold SST bias of about 1.5°C over the northern tropical Atlantic, and a warm bias of about 2.5°C over the eastern equatorial region. Unfortunately, these SST biases are not significantly improved in CM2.5. Although the warm SST bias in the Angola-Benguela Area is

reduced by about 0.5°C in CM2.5 relative to CM2.1, a warm SST bias of about 4.5°C persists there. Through we only show comparison to the ERSSTv3b, these SST biases are almost same relative to the HadISST data.

The largest bias of the annual mean SST in CM2.1 and CM2.5 is a warm SST bias over the eastern equatorial region, which is also present in almost all CMIP3 climate models, particularly in boreal summer. Therefore, we explore boreal spring wind biases to assess the sources of the warm SST bias. Richter and Xie (2006) and Richer et al. (2010) showed that the warm SST bias has been attributed to a bias towards weak easterly equatorial wind in boreal spring, which drives the excessively warm SST and deep thermocline in the eastern equatorial region and is amplified through the Bjerknes positive feedback (Bjerknes 1969). As shown in Table 1a, the easterly trade wind stress along the equator in CM2.1 is only 25% of the observed wind stress in boreal spring. This bias in boreal spring trade wind is partially reduced in CM2.5, but the simulated easterly is still only half of the observed wind stress. Associated with the warm SST bias and weak easterly equatorial wind, the mixed-layer depth in the southeastern tropical Atlantic is deeper by 10m in CM2.1 and CM2.5 than observations (figure not shown). Interestingly, the atmospheric components of CM2.1 and CM2.5 forced by observed SST can capture reasonable strength of the observed easterly wind stress, suggesting that these weak wind biases arise from coupled processes. The southerly winds in the southeastern tropical Atlantic may also contribute to the warm SST bias because the southerly winds induce cold upwelled water along the West African coast in the South Hemisphere, that extends westward by

advection and Rossby wave propagation, and cools the eastern equatorial SST (Philander and Pacanowski 1981). The southerly winds along the West African coast are also much weaker in CM2.1 and CM2.5 relative to observation (Table 1b). The southerly wind stress in CM2.1 is only 20% of the observed wind stress. This bias is marginally reduced in CM2.5, but yet captures only 30% of the observed wind stress. The weak bias of southerly winds appeared in CM2.1 and CM2.5 is also ubiquitous in the IPCC-AR4 CMIP3 climate models (Doi et al. 2010). The atmospheric components of two coupled models forced by observed SST already show the weak southerly winds along the West African coast at only 50% of those observed. Therefore, the improvement of the weak bias of southerly winds stress in AGCMs may be a good step towards reducing the warm SST bias in the southeastern tropical Atlantic, as we further discuss in Section 5.

Although the most serious SST biases are not improved by the differences between CM2.1 and CM2.5, the annual mean precipitation field is substantially improved in CM2.5 relative to CM2.1. Over the northern South America, CM2.1 shows a deficient rainfall relative to observations, while CM2.5 simulates a considerably more reasonable rainfall distribution (Fig 2 and Table 1c). It is noteworthy that regions that become rainier in CM2.5 relative to CM2.1 are associated with the steeper topography in high mountain regions (Fig. 2d). Therefore we hypothesize that the higher resolution of CM2.5 allows for these orographic features (and their impacts) to be better captured, while the low resolution in CM2.1 results in smoother topography. Consistent with this hypothesis, the improvement in northern

South American rainfall is also evident in atmosphere-only models: high-resolution AM2.5 with LM3 (or LM2) shows more rainfall over the northern South America than the coarse-resolution AM2.1 (figure not shown).

Rainfall in the Congo basin is well simulated in both CM2.1 and CM2.5 (Table 1d). Given the results of Richter et al. (2011) and the suggestion of Wahl et al. (2011), we expected some improvement of the equatorial zonal winds and the zonal SST gradient from improving the precipitation pattern between the northern Brazil and the Congo. The winds are, indeed, marginally improved in CM2.5. However, this is not sufficient to correct the mean state SST bias. Note that CM2.5 shows an excessive precipitation bias associated with the marine Atlantic ITCZ in 50°-20°W, which is associated with the 0.5°C warmer mean SST in CM2.5 relative to CM2.1 (Fig. 1c and Fig. 2).

The annual cycle of the rainfall over the Sahel and the northern South America is shown in Figure 3. In CM2.1, there is excessive rainfall (by 40%) in the Sahel, while rainfall over northern South America is deficient – particularly in boreal summer. Boreal summer rainfall over the northern South America in CM2.1 is only 20% of that observed. Meanwhile, the annual cycle of the rainfall over the Sahel and the northern South America is drastically improved in CM2.5. This marked improvement in CM2.5 is associated with a significant reduction of some biases in the seasonal meridional migration of the ITCZ (Fig. 4). In CM2.1, the ITCZ shows an excessively large northward migration in boreal summer: the simulated ITCZ in CM2.1 is located around 3°S in boreal spring and moves northward to 12°N in boreal

summer, while the observed ITCZ in boreal spring around the equator and in boreal summer around 9°N. In CM2.5, the spring location of the ITCZ is around 2°S and its summer location is around 9°N, bringing its meridional migration more in line with that observed relative to CM2.1. The excessive southward migration bias of the ITCZ in CM2.1 and CM2.5 during January-March is associated with the weak bias of southerly winds stress along the West African coast (Table 1b).

The excessive northward migration bias of the ITCZ in CM2.1 during boreal summer is linked with the seasonal variation of the SST and the subsurface Guinea Dome region in northeastern tropical Atlantic, a region where seasonal variations of SST are large. In June, the difference in the northeastern tropical Atlantic SST between CM2.1 and CM2.5 is very small and the maximum peaks of SST are located around 4ºN in CM2.1 and CM2.5 (Fig. 5a). However, we found the large difference in August (Fig. 5b). CM2.1 shows colder SST relative to CM2.5 and observation in 5-15ºN. As a result, CM2.1 shows double peaks of the SST and the maximum SST around 16ºN. This SST bias leads to the excessive northward migration bias of the ITCZ in CM2.1 in boreal summer.

To understand the mechanisms behind the annual cycle of the northeastern tropical Atlantic SST, we build a diagnostic mixed-layer heat budget (Appendix 1). The annual cycle of the SST in CM2.1 in boreal summer is significantly different from that in CM2.5 and observation. This difference can be largely understood in terms of the ocean dynamical contribution (Table 2). The cooling tendency from ocean

dynamics in boreal summer is due to subsurface doming of the thermocline in the northeastern tropical Atlantic, known as the Guinea Dome (or the Dakar Dome; Mazeika 1967). Fig. 6 shows the summer field of wind stress, Ekman upwelling, and ocean stratification around mixed-layer depth. Ekman upwelling is calculated by wind stress in observations and models. In the observational estimates, the Guinea Dome is climatologically located in 10°-15°N, 35°-20°W. The ocean stratification over the simulated dome in CM2.1 is four times stronger than observation, and the simulated dome in CM2.1 is located further north by 4°, and extends further westward relative to observation. The strong bias in the Ekman upwelling over the Guinea Dome in boreal summer influences the seasonal variation of the SST in this region. The mechanism is shown schematically in Fig. 7. The Guinea Dome develops from boreal spring through summer from the Ekman upwelling associated with the northward migration of the ITCZ (Siedler et al. 1992; Yamagata and Iizuka 1995; Doi et al. 2009), which cools the mixed-layer temperature through entrainment (Doi et al. 2010). This is consistent with the observational study of Yu et al (2006). CM2.1 overestimates the cooling tendency of the SST by the ocean dynamics associated with the cold subsurface Guinea Dome and strong Ekman upwelling. CM2.5 significantly improved those biases and successfully captures the coupled process among the northward migration of the ITCZ, the SST, and the subsurface Guinea Dome.

Although the equatorial region and the Angola-Benguela Area also show large seasonal variations in observation and two models, we focused on the northern tropical Atlantic in this paper, because the significant improvement in CM2.5 are found

in the northward migration of the Atlantic ITCZ. In contrast to the northern tropical Atlantic, the differences between CM2.1 and CM2.5 did not result in an improvement to the serious SST biases in the equatorial region and the Angola-Benguela Area (Fig. 1).

4. Interannual variation

Maps of the standard deviation of the interannual SST anomaly are shown in Figure 8. As in the seasonal variation of SST, there are three regions of large interannual variability, each of which has strong seasonal phase-locking of the variability (Fig. 9). Thus, interannual variations in these regions of the tropical Atlantic can be described as a modulation of the annual cycle. In this paper we focus on the seasonal phase-locking of the interannual variations of SST averaged in the NTA (Northern Tropical Atlantic: 35°-20°W, 5°-20°N), because CM2.5 shows a significantly reduced bias in the seasonal phase-locking of interannual variations in the NTA relative to CM2.1 (Fig. 9a). However, in the equatorial Atlantic (ATL3) and the Angola-Benguela Area (ABA), both CM2.1 and CM2.5 fail to simulate the seasonal phase-locking of the interannual variations of SST.

The observed standard deviation of the NTA SST anomaly develops from February, reaches its maximum peak in April, and decays abruptly from May through September. The observed standard deviation of the SST anomaly in September is smaller by about 50% than that in April. CM2.1 successfully simulates the

development phase of interannual anomalies from early winter through boreal spring. However, the standard deviation in CM2.1 keeps increasing through March-May, and the decay from June through August is substantially weaker than that observed. As a result, the interannual variations of August NTA SST in CM2.1 are stronger by about 65% relative to observations. This bias in the seasonal phase-locking of the interannual variation of the NTA SST is significantly reduced in CM2.5. Since the interannual variability of the NTA SST in boreal summer may impact on the Sahel rainfall, the West African monsoon, and Atlantic hurricane activity, the CM2.1 bias in the seasonal phase-locking of the interannual variations of the NTA SST could represent a serious limitation to seasonal predictions based on CM2.1. Therefore, we aim to understand its causes in CM2.1, and why this bias is improved in CM2.5.

We explore a composite analysis to help understanding the mechanism of the seasonal phase-locking of interannual variations of the NTA SST. We construct a composite by averaging, based on selecting warm (cold) SST years in the NTA, when the interannual SST anomaly in the NTA exceeds one standard deviation during the mature season of March-May. The details are shown in Table 3. We have about 1.5 year per decade as a composite year in observations and models.

In observations, positive SST anomalies develop in the NTA from early winter through April and the warming tendency is strongest in February (figure not shown), mainly due to the surface enthalpy flux contribution, $\frac{Q - q_{sw}}{\rho C_p H_{mix}}$, (Table 4). This feature is well simulated in CM2.1 and CM2.5. We note that interannual variations of

surface enthalpy flux contribution, $\frac{Q - q_{sw}}{\rho C_p H_{mix}}$ (see Appendix-1), include not only interannual variations of surface enthalpy flux, but also interannual variations of mixed-layer depth (e.g. Morioka et al 2010; 2012). However, we have confirmed that interannual variations of mixed-layer depth do not contribute to $\frac{Q - q_{sw}}{\rho C_p H_{mix}}$ over the northern tropical Atlantic in boreal spring, and interannual variations of surface enthalpy flux Q are dominant (figure not shown). All observational datasets, CM2.1, and CM2.5 show wind-induced latent heat flux anomaly as the dominant term in the net surface enthalpy flux anomaly (Table 4). The composites of the latent heat flux and wind stress anomalies in February (Fig. 10) suggest that the warming mechanism is consistent with the WES positive feedback (Xie 1999). The WES feedback is associated with the southwesterly wind anomaly and weaker trade winds in the northern tropics. Those wind anomalies result in less evaporation and thus suppressed latent heat loss from ocean, leading to warmer SST in the northern tropical Atlantic. The dominance of this mechanism in the growth of SST anomalies in the northern tropical Atlantic has been discussed in previous works (Carton et al. 1996; Chang et al. 1997; Xie 1999; Huang and Shukla 2005; Hu et al. 2008; Lin et al. 2008). We confirmed that CM2.1 and CM2.5 reasonably capture the WES feedback and there are no significant difference between CM2.1 and CM2.5 (Fig. 10), although some biases are found in two models. In two models, the strongest warming area is about 4° southward of that in observations. This may be due to the southerly ITCZ location bias during boreal winter-spring in mean climatology, as discussed in section 3.

Although the essence of the boreal spring development mechanism is reproduced in both CM2.1 and CM2.5, the boreal summer decay mechanism is incorrectly represented in CM2.1. In August of the warm NTA years, the difference in the northeastern tropical Atlantic SST between CM2.1 and CM2.5 is much larger relative to February. The largest difference in SST anomalies between CM2.1 and CM2.5 is located around in 8º-12ºN in August (Fig. 11), where the Guinea Dome is located in early summer. In this region, rate of change of the SST anomaly in CM2.1 is different from observation and CM2.5: CM2.1 shows that the warming tendency of the SST is stronger from February through May. In particular, during April, the positive SST anomaly in CM2.1 still develops strongly, while the SST anomalies in the observations and CM2.5 start to decay in April. We explored the diagnostic mixed-layer heat budget anomaly in this region (Eq. A2 in Appendix, Table 5). Although there are substantial discrepancies between the observational datasets, the NCEP/NCAR reanalysis data indicates that the ocean dynamical contribution plays an important role on the summer decay. Some previous works suggested that the ocean dynamical cooling counteracts the warming by the WES feedback and provides an important negative feedback that helps to terminate warm events (Joyce et al 2004; Lee and Wang 2008; Doi et al. 2009; Doi et al. 2010; Mahajan et al. 2010). However, CM2.1 fails to simulate the cooling effect by the ocean dynamical contribution and shows the warming tendency by the ocean dynamical contribution. Therefore, the peak season of the SST anomaly moves from boreal spring into early summer and the warm SST anomaly is sustained through late summer in CM2.1. The bias in the ocean dynamical

contribution is significantly reduced in CM2.5

Why does CM2.1 fail to simulate the decay mechanism by the ocean dynamical contribution in boreal summer? In large part, the answer lies in the inability of CM2.1 to capture the negative feedback associated with the Guinea Dome. In the diagnostic mixed-layer heat budget anomaly of Table 5, the vertical entrainment contribution induced by the entrainment rate anomaly and climatological ocean stratification, $(w_{ent})' * \left(\frac{\overline{T_{mld} - T_d}}{H_{mix}} \right)$ (Appendix 2), can explain about 80% of the CM2.1 bias of the warming tendency during boreal early summer. As discussed above, the warm SST anomalies in the NTA is associated with an anomalously northward migration of the ITCZ, which leads to the positive wind stress curl anomaly and strong Ekman upwelling anomaly over the climatological Guinea Dome region. Therefore, enhanced upwelling plays an important role on the termination of the warm SST anomaly in the NTA through entrainment (schematic diagram: Fig. 18 of Doi et al. 2010). Observations show the Ekman upwelling anomaly in 6º-15ºN over the climatological Guinea Dome region associated with the northward migration of the ITCZ (Figs. 12a and 13). However, in CM2.1, there is a downwelling Ekman anomaly in 3º-15ºN (Figs. 12b and 13). This disagreement as to the sign of the wind-induced vertical velocity in 3º-15ºN between observations and CM2.1 is due to the climatological mean difference in the location of the ITCZ and the characteristic of Ekman upwelling around the ITCZ. In the mean climatology, CM2.1 shows the stronger Ekman upwelling and the broader zone of Ekman upwelling in 6º- 18ºN

around the simulated ITCZ relative to observation (Fig. 13).

The CM2.1 bias for an excessive seasonal northward migration of the ITCZ in CM2.1 from boreal spring to summer (discussed in Section 3) is amplified in interannual timescale, and results in the Ekman upwelling anomaly further north around 18°-25°N and the Ekman downwelling anomaly in 3º-15ºN. The downwelling anomaly over the strong doming of thermocline results in persistent warm SST anomalies in CM2.1 in 8º-12ºN during August. This incorrect oceanic role associated with the subsurface ocean in CM2.1 is significantly improved in CM2.5 in part because the seasonal meridional migration of the ITCZ and the Ekman upwelling in the northern tropical Atlantic is well simulated (Figs. 12 and 13). Note that the centers of the simulated domes in warm NTA years in CM2.1 and CM2.5 are similar to the mean climatologies in CM2.1 and CM2.5, because anomalies of ocean stratification around mix-layer depth are less than 5% of the mean climatology. Recovering the correct seasonal meridional migration of the Atlantic ITCZ is key not only for the mean annual cycle, but also for the seasonal phase-locking of the interannual variations of the NTA SST.

The cold years of the NTA SST can be explained by using similar mechanisms of opposite sign to the warm years, although there are some differences in the effectiveness of the entrainment cooling and statistical significance. Because of page limits, relevant figures are not shown in this paper.

5. Discussions and summary

Using output from the "1990 Control" simulations of two coupled GCMs (CM2.1 and the high-resolution CM2.5), the tropical Atlantic biases in the mean state, the annual cycle, and the interannual variations were investigated. Many aspects of the simulation are improved in CM2.5–yet others persist. The mean annual cycle of rainfall over the Sahel and the northern South America are well simulated in CM2.5, while CM2.1 shows the excessive rainfall over the Sahel and the deficient rainfall over northern South America particularly in boreal summer. Improvements in simulation of rainfall in CM2.5 are tied to a more realistic meridional migration of the model's ITCZ. In CM2.1, the meridional migration of the ITCZ is larger than observed.

The biases in the meridional migration of the ITCZ in CM2.1 arise from a coupled evolution of SST, Ekman upwelling velocity, and the subsurface Guinea Dome. The Guinea Dome develops from late boreal spring through summer and matures in boreal autumn driven by the wind-induced Ekman upwelling associated with the northward migration of the ITCZ. CM2.1 shows excessive Ekman upwelling and the enhanced Guinea Dome associated with further northward migration of the ITCZ. Entrainment cooling over the Guinea Dome plays an important role on the seasonal variation of the upper SST from boreal summer through autumn. CM2.5 produces an improved local wind-induced Ekman upwelling and oceanic stratification over the Guinea Dome in boreal summer. The coupled process connecting the ITCZ, SST, and the subsurface Guinea Dome strongly influence on the seasonal dependence of the interannual variations of SST in the northern tropical Atlantic.

The interannual SST anomaly in the northern tropical Atlantic develops from early boreal winter through spring, and reaches the maximum in April in observations. There are no gross differences in the simulation of the development mechanism between CM2.1 and CM2.5. However, the mechanisms for summer decay of NTA interannual variability is not well simulated in CM2.1. CM2.1 shows persistent warm SST anomalies in 8º-12ºN through August in the warm NTA years, when observations show no significant SST anomalies. The bias in the summer decay phase of the interannual SST anomaly in CM2.1 is mainly due to the ocean dynamical contribution by the subsurface Guinea Dome. In observational estimates, warm SST anomalies over the subsurface Guinea Dome are reduced by a negative feedback tied to the Guinea Dome (Doi et al. 2010): an anomalously northward migration of the ITCZ associated with the warm SST anomaly in the northern tropical Atlantic leads to cyclonic wind stress curl anomaly, and thus enhanced Ekman upwelling over the Guinea Dome region. This coupled evolution plays a critical role on the summer decay of the warm SST anomaly through entrainment cooling (schematic diagram is shown in Fig. 14a). This mechanism is also interpreted as an enhanced annual cycle shown in Fig.7. However, CM2.1 fails to simulate this negative feedback. In CM2.1, the climatological ITCZ is located to the north of that observed, and it shows excessive Ekman upwelling and broad zone of Ekman upwelling in 6º–18ºN around the simulated ITCZ. These characteristics lead to an Ekman upwelling anomaly in 18º-25ºN and the Ekman downwelling anomaly in 3º-15ºN during warm NTA periods. The Ekman downwelling anomaly over the strong doming of thermocline sustains the warm SST anomaly in 8º-

12ºN through August (Fig. 14b).

Meanwhile, CM2.5 successfully reproduces the seasonal phase-locking of the interannual variations of the northern tropical Atlantic SST. This is due to a more realistic climatological meridional migration of the ITCZ in CM2.5, which leads to a more realistic positioning and strength of the Guinea Dome. This improved mean state provides a background for a more realistic decay of interannual anomalies in the northern tropical Atlantic. The coupled processes that connect northward migrations of the ITCZ, SST, and the subsurface Guinea Dome are key to understand the Tropical Atlantic Variability.

We hypothesize that CM2.5 may exhibit better prediction skill of northern Atlantic climate conditions and their impacts than CM2.1, because CM2.5 more successfully reproduces the annual mean and the annual cycle of the rainfall over the Sahel and the northern South America, the subsurface Guinea Dome variations, and the seasonal phase-locking of the interannual variations of the northern tropical Atlantic. Since the seasonal phase locking of anomalies in the NTA is key to its influence on seasonal phase-locked phenomena (*e.g.*, tropical cyclone activity), we hypothesize that the experimental predictions of seasonal hurricane activity described in Vecchi et al. (2011), which have been based in part on predictions of the NTA using CM2.1, will be improved by using CM2.5.

Differences between CM2.1 and CM2.5 are not only horizontal resolution, but also include some changes to parameterizations, numerics, and the land-model. At this stage, we cannot confidently assess whether increased resolution or changes to

numerics and land model have been dominant in reducing the biases in precipitation and the ITCZ in CM2.5. Sensitivity experiments for exploring this question are being conducted as part of our current research activities.

Meanwhile, the differences between CM2.5 and CM2.1 did not lead to reductions in very large SST biases in the eastern equatorial region and Angola-Benguela Area, which are found in almost all CMIP3 models (Richter and Xie 2008). Both the annual cycle and the interannual variations of SST in these two areas are stronger in both models than in observations. In addition, neither model can simulate the seasonal phase-locking of the interannual variations of SST over the Angola-Benguela Area. Therefore, neither model realistically simulates the Atlantic Niño and the Benguela Niño, which are two major climate modes in the tropical Atlantic. A tendency for the weak southerly winds along the southwestern African coast already appears in the atmospheric components of these coupled models when forced with observed SST (Table 1), suggesting that atmospheric biases are likely causative factors for the emergent coupled biases. The weak bias of southerly winds stress along the West African coast is associated with the excessive southward migration bias of the ITCZ in CM2.1 and CM2.5 during boreal winter-spring. At this stage, we speculate that the problems are mostly related to atmospheric physics associated with deep convection and cloud processes in the AGCM. Sensitivity experiments for reducing the tropical Atlantic biases are also being conducted as part of GFDL's research program.

In this paper, we have focused on the tropical Atlantic basin. However, uncertainty still remains as to remote effects of the Pacific, the mid-latitude Atlantic,

the tropical southern Atlantic on climate conditions in the tropical Atlantic (see reviews by Xie and Carton 2004; Chang et al. 2006). In particular, Czaja (2004) suggested that the seasonal dependence of the interannual variability in the northern tropical Atlantic is a reflection not only of local air-sea coupling, but also the remote forcing by the North Atlantic Oscillation and the ENSO. Although the amplitude of the Pacific ENSO is stronger in CM2.1 than that in observations (Wittenberg et al. 2006), this bias is partially reduced in CM2.5 (Delworth et al. 2012). Exploring the relation between the tropical Atlantic and other basins is also underway.

Acknowledgments

We thank to Drs. Andrew Wittenberg, Stephen Griffies, Rong Zhang, Gabriel Lau, Rym Msadek, Ian Lloyd, Syukuro Manabe, Bruce Wyman for helpful comments and suggestions. We are grateful to the GFDL-CM2.1 and CM2.5 modeling services team for their assistance with model infrastructure support and data processing.

Appendix: Mixed-layer heat budget analysis

We explore the diagnostic bulk mixed-layer heat budget:

$$\frac{\partial T_{mix}}{\partial t} = \frac{Q - q_{sw}}{\rho C_p H_{mix}} + ocean\ dynamics\ contribution\ . \quad \text{(A1)}$$

Here, T_{mix} is the mixed-layer temperature, a proxy for SST, ρ is the typical sea water density (1025 kg m^{-3}), C_p is the typical heat capacity of the sea water (3996 J kg^{-1} K^{-1}), and H_{mix} is the mixed-layer depth, which is calculated as the depth at which the potential density becomes 0.125 kg m^{-3} larger than the surface density, as used by Levitus (1982). The quantity Q denotes the net surface enthalpy flux, and q_{sw} is the downward solar insolation that penetrates through the bottom of the mixed-layer. Thus, the first term on the right hand side represents the influence of atmospheric thermal forcing. The ocean dynamical contribution is simply estimated by difference between rate of change of the mixed-layer temperature and the surface enthalpy flux contribution.

To understand the detailed ocean dynamical contribution in the Guinea Dome region, we explore the detailed mixed-layer heat budget:

$$\frac{\partial T_{mix}}{\partial t} = \frac{Q - q_{sw}}{\rho C_p H_{mix}} - W_{ent}\frac{T_{mix} - T_e}{H_{mix}} - U \cdot \nabla T_{mix} + residual\ . \quad \text{(A2)}$$

The second term on the right hand side represents the oceanic cooling associated with entrainment, where W_{ent} is the entrainment rate, and T_e is the temperature of water entrained into the mixed-layer and assumed to be the temperature 5 m below the mixed-layer (e.g. Qu et al. 2001). The entrainment rate can be assumed by

$$W_{ent} = \frac{\partial H_{mix}}{\partial t} + W_{mb} + U \cdot \nabla H_{mix}, \quad \text{(A3)}$$

where $\frac{\partial H_{mix}}{\partial t}$ denotes the rate of change of the mixed-layer depth, W_{mb} is the vertical velocity at the base of the mixed-layer, and $U \cdot \nabla H_{mix}$ is the horizontal transport. If W_{ent} is negative, we assume W_{ent}=0. This estimation of the oceanic entrainment cooling is a well-known diagnostic method (e.g. Hagos and Cook 2009). The third term, $U \cdot \nabla T_{mix}$, represents the horizontal heat transport in the mixed-layer.

References

Adler, R.F., and Coauthors, 2003: The version 2 Global Precipitation Climatology Project (GPCP) monthly precipitation analysis (1979-Present). *J. Hydrometeor.*, **4,** 1147-1167.

Bjerknes, J., 1969: Atmospheric teleconnections from the equatorial Pacific. *Mon. Wea. Rev.,* **97**,163-172.

Carton, J. A., and B. Huang, 1994: Warm events in the tropical Atlantic. *J. Phys. Oceanogr.*, **24,** 888-903.

Carton, J. A., X. Cao, B. S. Giese, and A. M. da Silva, 1996: Decadal and interannual SST variability in the tropical Atlantic Ocean. *J. Phys. Oceanogr.*, **26**, 1165-1175.

Chang, P., L. Ji, and H. Li, 1997: A decadal climate variation in the tropical Atlantic ocean from thermodynamic air-sea interactions. *Nature,* **385,** 516-518.

Chang, P., and Coauthors, 2006: Climate fluctuations of tropical coupled system –the role of ocean dynamics. *J. Climate*, **19,** 5122-5174.

Czaja, A., 2004: Why is North Tropical Atlantic SST variability stronger in boreal spring? *J. Climte*, **17,** 3017-3025.

Davey, M. K., and coauthors, 2002: STOIC: a study of coupled model climatology and variability in tropical ocean regions. *Climate Dyn.,* **18**, 403-420.

Delworth, T. L., and Coauthors, 2006: GFDLs CM2 global coupled climate models. Part Ⅰ: Formulation and simulation characteristics. *J. Climate*, **19,** 643-674.

Delworth, T. L., and Coauthors, 2011: Simulated climate and climate change in the

GFDL-CM2.5 high-resolution coupled climate model. *Submitted to J. Climate*.

Doi, T., T. Tozuka, H. Sasaki, Y. Masumoto, and T. Yamagata, 2007: Seasonal and interannual variation of oceanic conditions in the Angola Dome, *J. Phys. Oceanogr.,* **37,** 2698-2713.

Doi, T., T. Tozuka, and T. Yamagata, 2009: Interannual variability of the Guinea Dome and its possible link with the Atlantic Meridional Mode. *Climate Dyn.*, **33**, 985-998.

Doi, T., 2009: Tropical Atlantic climate modes and their links with upwelling domes. Ph.D. thesis, the University of Tokyo, 141 pp.

Doi, T., T. Tozuka, and T. Yamagata, 2010: The Atlantic Meridional Mode and its coupled variability with the Guinea Dome. *J. Climate*, **23,** 455-475.

Dommenget, D., V. Semenov, and M. Latif, 2006: Impacts of the tropical Indian and Atlantic Oceans on ENSO, *Geophys. Res. Lett.*, **33**, doi:10.1029/2006GL025871.

Emanuel, K., 2005: Increasing destructiveness of tropical cyclones over the past 30 years. *Nature*, **436,** 686-688.

Farneti, R., T. L. Delworth, A. J. Rosati, S. M. Griffies, F. Zeng, 2010: The role of mesoscale eddies in the rectification of the Southern Ocean response to climate change. *J. Phys. Oceanogr.*, **40**, 1539–1557.

GAMDT, 2004: The new GFDL global atmosphere and land model AM2/CM2.0: Evaluation with prescribed SST simulations. *J. Climate*. **17**, 4641–4673.

Gent, P.R., and J. C. McWilliams, 1990: Isopycnal mixing in ocean circulation models. *J. Phys. Oceanogr.*, **20**, 150–155.

Gnanadesikan, A., and Coauthors, 2006: GFDL's CM2 global coupled climate models.

Part II: The baseline ocean simulation. *J. Climate*, **19,** 675–697.

Griffies, S. M., 1998: The Gent-McWilliams skew flux. *J. Phys. Oceanogr.*, **28**, 831-841.

Griffies, S. M., A. Guanadesikan, R. C. Pacanowski, V. D. Larichev, J. K. Dukowicz, and R. D. Smith, 1998: Isoneutral diffusion in a z-coordinate ocean model. *J. Phys. Oceanogr.*, **28**, 805–830.

Griffies, S. M., and Coauthors, 2005: Formulation of an ocean model for global climate simulations. *Ocean Sci.,* **1.** 45-79.

Griffies, S. M., 2010: Elements of MOM4p1. *GFDL OCEAN GROUP TECHNICAL REPORT NO. 6*, p444.

Griffies, S. M., and coauthors, 2012: GFDL's CM3 Coupled climate model: characteristics of the ocean and sea ice simulations. *Journal of Climate, in press*.

Grodsky, S. A., J. A. Carton, S. Nigam, and Y. M. Okumura, 2012: Tropical Atlantic biases in CCSM4. *J. Climate*, in press.

Hagos, S. M., and K, H. Cook, 2009: Development of a coupled regional model and its application to the study of interactions between the West African monsoon and the eastern tropical Atlantic Ocean. *J. Climate*, **22**, 2591-2604.

Hu, Z.-Z., B. Huang, and K. Pegion, 2008: Leading patterns of the tropical Atlantic variability in a coupled general circulation model. *Climate Dyn.,* **30**, 703-726.

Huang, B., and J. Shukla, 2005: Ocean-atmosphere interactions in the tropical and subtropical Atlantic ocean. *J. Climate*, **18,** 1652-1672.

Joyce, T. M., C. Frankignoul, J. Yang, and H. E. Phillips, 2004: Ocean response and

feedback to the SST dipole in the Tropical Atlantic. *J. Phys. Oceanogr.,* **34**, 2525-2540.

Kalnay, E., and Coauthors, 1996: The NCEP/NCAR 40-year reanalysis project. *Bull. Amer. Meteor. Soc.,* **77,** 437-471.

Knutson, T. R., and Coauthors, 2006: Assessment of Twentieth-Century Regional Surface Temperature Trends Using the GFDL CM2 Coupled Models. *J. Climate*, **19**, 1624–1651.

Kucharski, F., I.-S. Kang, R. Farneti, and L. Feudale, 2011: Tropical Pacific response to 20th century Atlantic warming, *Geophys. Res. Lett.*, **38**, doi:10.1029/2010GL046248.

Large, W. G., J. C. McWilliams, and S. C. Doney, 1994: Oceanic vertical mixing: A review and a model with a nonlocal boundary layer parameterization. *Rev. Geophys.*, **32,** 363-403.

Lee, S.-K. and C. Wang, 2008: Tropical Atlantic decadal oscillation and its impact on the equatorial atmosphere-ocean dynamics: A simple model study. *J. Phys. Oceanogr.,* **38,** 193-212.

Levitus, S., 1982: Climatological Atlas of the World Ocean, NOAA Professional Paper 13, U.S. Department of Commerce.

Lin, S-J., 2004: A "vertically Lagrangian" finite-volume dynamical core for global models. *Mon. Wea. Rev.,* **132,** 2293-2307.

Lin J, Han W, and Lin X., 2008: Observational analysis of the wind-evaporation-SST feedback over the tropical Pacific Ocean. *Atmos. Sci. Lett.,* **9,** 231-236**.**

Lloyd, I. D., and G. A. Vecchi, 2011: Observational evidence for oceanic controls on Hurricane intensity. *J. Climate,* **24**, 1138–1153.

Locarnini, R.A., A.V. Mishonov, J.I. Antonov, T.P. Boyer, H.E. Garcia and S. Levitus, 2006: World Ocean Atlas 2005, Volume 1: Temperature. S. Levitus. *NOAA Atlas NESDIS 61, U.S. Government Printing Office, Washington, D.C.Äi0: 182.*

Look, A. P., A. R. Brown, M. R. Bush, G. M. Martin, and R. N. B. Smith, 2000: A new boundary layer mixing scheme. Part Ⅰ: Scheme description and single-column model tests. *Mon. Wea. Rev.,* **128,** 3187-3199.

Lu, J., and T. L. Delworth, 2005: Oceanic forcing of the late 20th century Sahel drought. *Geophys. Res. Lett.,* **32**, doi:10.1029/2005GL023316.

Mazeika, P. A., 1967: Thermal domes in the eastern tropical Atlantic Ocean. *Limnol. Oceanogr.,* **12,** 537-539.

Meehl, G. A., and coauthors, 2007: The WCRP CMIP3 multimodel dataset - A new era in climate change research. *Bull. Amer. Meteor. Soc.,* **88,** 1383-1394.

Milly, P. C. D., S. L. Malyshev, E. Shevliakova, K. A. Dunne, K. L. Findell, K. Eng, T. Gleeson, Z. Liang, P. Phillips, R. J. Stouffer, and S. Swenson. Enhanced Representation of Land Physics for Earth-System Modeling. *in preparation.*

Moorthi, S., and M. J. Suarez, 1992: Relaxed Arakawa-Schubert: A parameterization of moist convection for general circulation models. *Mon. Wea. Rev.,* **120,** 978-1002.

Morioka, Y., T. Tozuka, and T. Yamagata, 2010: Climate variability in the Southern Indian Ocean as revealed by Self-Organizing Maps. *Climate Dyn.*, **35**, 1075-1088.

Morioka, Y., T. Tozuka, and T. Yamagata, 2012: On the growth and decay of the

subtropical dipole mode in the South Atlantic. *J. Climate*, in press.

Muñoz, E., W. Weijer, S. Grodsky, and I. Wainer, 2012: Mean and Variability of the Tropical Atlantic Ocean in the CCSM4. *J. Climate*, in press.

Philander, S. G. H., and R. C. Pacanowski, 1981: The oceanic response to cross-equatorial winds (with application to costal upwelling in low latitudes). *Tellus,* **33**, 201-210.

Putman, W M., and Shian-Jiann Lin, 2007: Finite-volume transport on various cubed-sphere grids**.** *J. Computational Phys*., **227**, 55-78.

Qu, T., H. Mitsudera, and B. Qiu, 2001: A climatology of the Kuroshio/Oyashio system east of Japan. *J. Phys. Oceanogr.,* **31,** 2575-2589.

Rayner, N. A., and Coauthors, 2003: Global analyses of sea surface temperature, sea ice, and night marine air temperature since the late nineteenth century. *J. Geophys. Res.,* **108**, doi:10.1029/2002JD002670.

Richter, I., and S. P. Xie, 2008: On the origin of equatorial Atlantic biases in coupled general circulation models. *Climate Dyn.,* **31**, 587-598.

Richter, I., S. P. Xie, A. T. Wittenberg, and Y. Masumoto, 2011: Tropical Atlantic biases and their relation to surface wind stress and terrestrial precipitation. *Climate Dyn.,* in press.

Russell, J. L., R. J. Stouffer, and K. W. Dixon, 2006: Intercomparison of the Southern Ocean Circulations in IPCC Coupled Model Control Simulations. *J. Climate*, **19**, 4560–4575.

Servain, J., 1991: Simple climatic indices for the tropical Atlantic-ocean and some

applications. *J. Geophys. Res.,* **96,** 15137-15146.

Siedler, G., N. Zangenberg, and R. Onken, 1992: Seasonal changes in the tropical Atlantic circulation: observation and simulation of the Guinea Dome. *J. Geophys. Res.,* **97,** 703-715.

Shevliakova E, Pacala S, Malyshev S, Hurtt G, Milly P, Caspersen J, Sentman L, Fisk J, Wirth C, Crevoisier C. 2009. Carbon cycling under 300 years of land use change: Importance of the secondary vegetation sink. *Global Biogeochemical Cycles* **23**, doi:10.1029/2007GB003176.

Simmons, A. J. J. K. Gibson, 2000: The ERA-40 Project Plan. In: The ERA-40 Project Report Series, Nr. 1. http://www.ecmwf.int/research/era/Project/Plan/index.html.

Smith, T. M., R. W. Reynolds, T. C. Peterson, J. Lawrimore, 2008: Improvements to NOAA's Historical Merged Land–Ocean Surface Temperature Analysis (1880–2006). *J. Climate*, **21,** 2283-2296.

Stockdale, T. N., M. A. Balmaseda, and A. Vidard, 2006: Tropical Atlantic SST prediction with coupled ocean-atmosphere GCMs. *J. Climate*, **19**, 6047-6061.

Stouffer R. J., and Coauthors, 2006: GFDL's CM2 global coupled climate models. Part IV: Idealized climate response. *J. Climate,* **19,** 723–740.

Sutton R. T., and D. L. R. Hodson, 2005: Atlantic Ocean forcing of North American and European summer climate. *Scinece*, **309**, 115-118.

Sweeney, C., A. Gnanadesikan, S. M. Griffies, M. J. Harrison, A. J. Rosati, and B. L. Samuels, 2005: Impacts of shortwave penetration depth on large-scale ocean

circulation and heat transport. *J. Phys. Oceanogr.,* **35,** 1103-1119.

Tozuka, T., T. Miyasaka, A. Chakraborty, M. Mujumdar, S. K. Behera, Y. Masumoto, H. Nakamura, and T. Yamagata, 2006: University of Tokyo Coupled General Circulation Mode (UTCM1.0). *Ocean-atmosphere research report No. 7.*

Tozuka, T., T. Doi, T. Miyasaka, N. Keenlyside, and Toshio Yamagata, 2011: How to simulate the equatorial Atlantic zonal SST gradient realistically in a coupled GCM. *J. Geophys. Res.,* **116**, doi:10.1029/2010JC006717.

Vecchi, G. A., and B. J. Soden, 2007: Effect of remote sea surface temperature change on tropical cyclone potential intensity. *Nature*, **450**, 1066-1070.

Vecchi, G. A., M. Zhao, G. Villarini, A. Rosati, I. Held, and R. Gudgel, 2011: Hybrid statistical-dynamical predictions of seasonal Atlantic hurricane activity. *Mon. Wea. Rev.,* **139**, 1070-1082.

Wahl, S., M. Latif, W. Park, and N. Keenlyside, 2011: On the Tropical Atlantic SST warm bias in the Kiel Climate Model. *Climate Dyn.*, **36,** 891-906.

Xie, P., and P. A. Arkin, 1997: Global precipitation: a 17-year monthly analysis based on qauge observations, satellite estimates, and numerical model outputs. *Bull. Amer. Meteor. Soc.*, **78**, 2539-2558.

Xie, S. P., 1999: A dynamic ocean-atmosphere model of the tropical Atlantic decadal variability. *J. Climate*, **12,** 64-70.

Xie, S. P., and J. A. Carton, 2004: Tropical Atlantic variability: patterns, mechanisms, and impacts. *Earth's Climate: The Ocean-Atmosphere Interaction: From Basin to Global Scales, Geophys. Monogr., Vol. 147, Amer. Geophys. Union*, 121-142.

Yamagata, T., and S. Iizuka, 1995: Simulation of the tropical thermal domes in the Atlantic: A seasonal cycle. *J. Phys. Oceanogr.,* **25,** 2129-2140.

Yu, L., X. Jin, and R. A. Weller, 2006: Role of net surface heat flux in seasonal variations of sea surface temperature in the tropical Atlantic Ocean. *J. Climate*, **19,** 6153-6169.

Zebiak, S. E., 1993: Air-sea interaction in the equatorial Atlantic region. *J. Climate*, **6,** 1567-1586.

Zhang, R., and. T. L. Delworth, 2006: Impact of Atlantic multidecadal oscillations on India/Sahel rainfall and Atlantic hurricanes. *Geophys. Res. Lett.*, **33**, doi:10.1029/2006GL026267.

Zhang, R., T. L. Delworth, and I. M. Held, 2007: Can the Atlantic Ocean drive the observed multidecadal variability in Northern Hemisphere mean temperature? *Geophys. Res. Lett.,* **34**, doi:10.1029/2006GL028683.

Tables

Table 1: Summary of boreal spring biases in CM2.1, CM2.5, and the atmosphere components of these models forced by observed SST. (a) The zonal wind stress along the Atlantic equator, averaged in 50°W-10°E, 2°S-2°N (N m^{-2}). Easterly wind is positive. (b) The meridional wind stress along the southeastern African coast, averaged in 5°-10°E, 10°S-0° (N m^{-2}). Southerly wind is positive. (c) The precipitation over northern South America, averaged in 75°-55°W, 10°S-10°N (mm day^{-1}). (d) The precipitation over the Congo basin, averaged in 10°W-40°E, 5°S-5°N (mm day^{-1}).

	Observations	CM2.1	CM2.5	AM2.1	AM2.5
(a) Easterly wind stress along the equator (N m^{-2})	0.014 (NCEP/NCAR) 0.016 (ERA40)	0.0033	0.0068	0.017	0.013
(b) Southerly wind stress along the African coast (N m^{-2})	0.033 (NCEP/NCAR) 0.030 (ERA40)	0.0061	0.0093	0.015	0.017
(c) Northern South America Rainfall (mm day^{-1}).	7.0 (CMAP) 7.9 (GPCP)	5.1	6.1	6.6	8.6
(d) Congo Rainfall (mm day^{-1}).	5.1 (CMAP) 4.8 (GPCP)	5.0	5.2	5.1	5.8

Table 2: The climatological mixed-layer heat budget averaged in the northern tropical Atlantic (35°-18°W, 5-15°N) in June-August (10^{-7} K s^{-1}). Each term is calculated as in Appendix-1. Observational estimates for rate of change of mixed-layer temperature, "Total", are from ERSSTv3 and HadISST datasets. Observational estimates for $\frac{Q - q_{sw}}{\rho C_p H_{mix}}$ are from NCEP/NCAR, ERA40, and OAFLUX datasets with the mixed-layer depth in WOA05.

	Total	$\frac{Q - q_{sw}}{\rho C_p H_{mix}}$	$W_{ent} \frac{T_{mix} - T_e}{H_{mix}}$	$(U \cdot \nabla T_{mix})$	Residual
Obs.	+1.53 ~ +1.61	+1.28 ~ +2.95	-	-	-
CM2.1	+0.88	+2.49	-2.14	-0.11	+0.64
CM2.5	+1.92	+2.73	-0.54	+0.19	-0.45

Table 3: Summary of the interannual variations of the Northern Tropical Atlantic SST in ERSSTv3, HadISST, CM2.1 and CM2.5 (NTA: 35°-18°W, 5°-20°N). (a) The standard deviations of the interannual variations of the northern tropical Atlantic SST in March-May, which is the seasonal maximum peak season of the interannual variations. (c) Warm years of the NTA SST used for a composite analysis. Also, the number of year per decade is shown. (d) Same as (c), but for cold years.

	Observation	CM2.1	CM2.5
(a) Standard Deviation in March-May	0.53 (ERSSTv3) 0.55 (HadISST)	0.57	0.51
(b) Warm year	8 years (66, 69, 70, 79, 80, 83, 87, and 88) 1.9 year/decade	38 years 1.3 year/decade	43 years 1.5 year/decade
(c) Cold year	5 years (68, 74, 85, 86, 89) 1.2 year/decade	39 years 1.3year/decade	37 years 1.3 year/decade

Table 4: Composite anomalies of the mixed-layer heat budget averaged in 50°-18°W, 10-20°N in Jan.-Mar. of warm NTA years (10^{-7} K s^{-1}). Positive (negative) value denotes ocean warming (cooling) tendency. Boldface shows values beyond 99% significance levels. (a) and (b) are calculated in Eq. 1 of Appendix-1. (c) is net surface enthalpy flux anomalies, (d) is latent heat flux anomalies, and (e) is wind speed-induced latent heat flux anomalies.

	(a) Total (10^{-7} K s^{-1})	(b) $\frac{Q - q_{sw}}{\rho C_p H_{mix}}$ (10^{-7} K s^{-1})	(c) Net. Hflx (W m^{-2})	(d) LH (W m^{-2}).	(e) LH-wind (W m^{-2}).
Obs.	**+0.59 ~ +0.67**	**+0.44 ~ +0.68**	**+11.2~ +15.9**	+8.6~ **+12.5**	**+14.9~ +21.9**
CM2.1	**+0.51**	**+0.68**	**+17.1**	**+13.5**	**+13.1**
CM2.5	**+0.63**	**+0.66**	**+17.2**	**+13.2**	**+13.4**

Table 5: Composite anomalies of the mixed-layer heat budget anomaly averaged in 40°-18°W, 8-12°N during March-July of the warm NTA years (10^{-7} K s^{-1}). Each term is calculated as in Appendix-1. Positive (negative) value denotes ocean warming (cooling) tendency. Boldface shows values beyond 99% significance levels.

	Total	$\frac{Q-q_{sw}}{\rho C_p H_{mix}}$	$(W_{ent})' * \left(\frac{\overline{T_{mix}-T_e}}{H_{mix}}\right)$	$(\overline{W_{ent}}) * \left(\frac{T_{mix}-T_e}{H_{mix}}\right)'$	$(U \cdot \nabla T_{mix})'$	Residual
Obs.	-0.049 ~ -0.20	+0.066 ~ -0.40				
CM2.1	**+0.17**	**-0.097**	**+0.21**	-0.022	+0.052	+0.029
CM2.5	**-0.096**	**-0.054**	+0.038	+0.031	-0.001	-0.11

Figure captions

Fig. 1: (a) Annual mean SST from the ERSSTv3 data (°C). The contour interval is 1°C. (b) Annual mean SST bias in CM2.1 from the ERSSTv3 data. The contour interval is 1°C. (c) Difference in annual mean SST between CM2.5 and CM2.1. The contour interval is 0.5°C. Note that the SST bias in CM2.1 and CM2.5 is almost same, if the HadISST dataset is used as a reference.

Fig. 2: (a) Annual mean rainfall from the CMAP data (mm day^{-1}). The contours interval is 2 mm day^{-1}. (b) Annual mean rainfall bias in CM2.1 from the CMAP data (mm day^{-1}). The contour interval is 2 mm day^{-1}. (c) Difference in annual mean rainfall between CM2.5 and CM2.1. The contours interval is 3 mm day^{-1}. (d) Difference in orography between CM2.5 and CM2.1 (m). The blue contour shows difference in annual mean rainfall between CM2.5 and CM2.1, same as (c). The Sahel region (20°W-10°E, 10°-20°N) and the northern South American region (75°-55°W, 10°S-10°N) are shown by solid boxes.

Fig. 3: (a) Seasonal cycle of rainfall averaged in the Sahel region (20°W-10°E, 10°-20°N) (mm day^{-1}). This index is also used in Lu and Delworth (2005). (b) Same as (a), but for the northern South American region: 75°-55°W, 10°S-10°N.

Fig. 4: (a) Seasonal meridional migration of the Atlantic ITCZ, which is defined as zero meridional wind stress averaged in 50°-20°W.

Fig. 5: Climatological SST averaged in the northeastern tropical Atlantic (35°-18°W) in (a) June and (b) August.

Fig. 6: (a) Climatology of wind stress (N m^{-2}; vector) and Ekman upwelling (shaded; 10^{-6} m s^{-1}) in July-September from the NCEP/NCAR reanalysis data. Upwelling is shown by blue shading, while downwelling is shown by red shading. (b) Climatology

of stratification around mixed-layer depth, $\frac{T_{mix}-T_e}{H_{mix}}$, averaged in July-September from the WOA05 data (10^{-2} K m^{-1}), (d) CM2.1 and (f) CM2.5. The contour interval is 0.2× 10^{-2}K m^{-1}. (c) Same as (a), but for CM2.1 bias and (e) CM2.5 bias from the NCEP/NCAR reanalysis data.

Fig. 7: Schematic diagram of the seasonal variations in the northern tropical Atlantic. (a) In boreal spring, surface enthalpy flux warms the SST and the mixed-layer depth is deep. (b) In boreal summer, the Guinea Dome develops through the Ekman upwelling associated with the northward migration of the ITCZ. The Guinea Dome cools the mixed-layer temperature through entrainment as a counteracting role of warming tendency by surface enthalpy flux.

Fig. 8: (a) Horizontal map of the standard deviation of the interannual SST anomaly averaged in whole season from the ERSSTv3 data, (b) CM2.1, and (c) CM2.5 (°C). Contour shows 0.2, 0.3, 0.4, 0.6, 0.9, and 0.13°C. The northern tropical Atlantic region (NTA: 35°-18°W, 5°-20°N), the Atlantic Niño index (ATL3: 20°W-0°, 3°S-3°N), and the Angola-Benguela area (ABA: 0°-20°E, 25°-5°S) are shown in boxes.

Fig. 9: (a) Monthly standard deviation of the interannual anomaly of SST from ERSSTv3 (bar), HadISST (grey line), GFDL-CM2.1 (red line), and CM2.5 (blue line) averaged in the northern tropical Atlantic region (NTA: 35°-20°W, 5°-20°N), (b) the Atlantic Niño index (ATL3: 20°W-0°, 3°S-3°N), (c) the Angola-Benguela region (ABA: 0°-20°E, 25°-5°S). We note that vertical scale in (b) is different from that in (a) and (c).

Fig. 10: (a) Composite anomalies for the latent heat flux from NCEP/NCAR reanalysis data in February of the warm NTA years (W m^{-2}). Positive values shows warming ocean. Contour interval is 5W m^{-2}. Color shading denotes anomalies above 90% significance level. (b) Same as (a), but for wind stress (N m^{-2}; vector). Red (blue) shading denotes negative (positive) wind stress anomalies above 90% significance. (c) Same as (a), but for CM2.1 and (e) CM2.5. Color shading denotes anomalies above 99% significance level. (d) Same as (b), but for CM2.1 and (f) CM2.5. Red (blue)

shading denotes weak (strong) anomalies above 99% significance.

Fig.11: Composite anomalies for SST averaged in 40º-18ºW in (a) February and (b) August of warm NTA years (ºC). The maximum bias in SST between observations and CM2.1 appears in 8º-12ºN during August.

Fig.12: (a) Composite anomalies for Ekman upwelling in March-July of warm NTA SST years from NCEP/NCAR reanalysis data (shaded; 10^{-6}m s^{-1}). Red (blue) shading denotes downwelling (upwelling) anomalies. Contour shows climatology of stratification around mixed-layer depth, $\frac{T_{mix}-T_e}{H_{mix}}$, in March-July from WOA05 data (10^{-2}K m^{-1}). Contour interval is 1×10^{-2}K m^{-1}. (b) Same as (a), but for CM2.1. (c) Same as (a) but for the differences between CM2.5 and CM2.1.

Fig. 13: (a) Climatology of ocean stratification around mixed-layer depth, $\frac{T_{mix}-T_e}{H_{mix}}$, averaged in 40º-18ºW during March-July (thick lines; K m^{-2}). Note that interannual anomalies in models are less than 5% of the mean values (dashed lines). (b) Composite anomalies for Ekman upwelling in 40º-18ºW during March-July in warm NTA years (10^{-6} m s^{-1}). Positive (Negative) values show downwelling (upwelling) anomalies. (c) Climatology of Ekman upwelling averaged in 40º-18ºW during March-July (10^{-6} m s^{-1}). Positive (Negative) values show downwelling (upwelling).

Fig.14: Schematic diagram for (a) the boreal summer decay mechanism of the warm SST in the northern tropical Atlantic linked with the Guinea Dome suggested by observational estimate and Doi et al. (2010). (b) The incorrect role of the Guinea Dome is found in CM2.1.

1 Fig.1

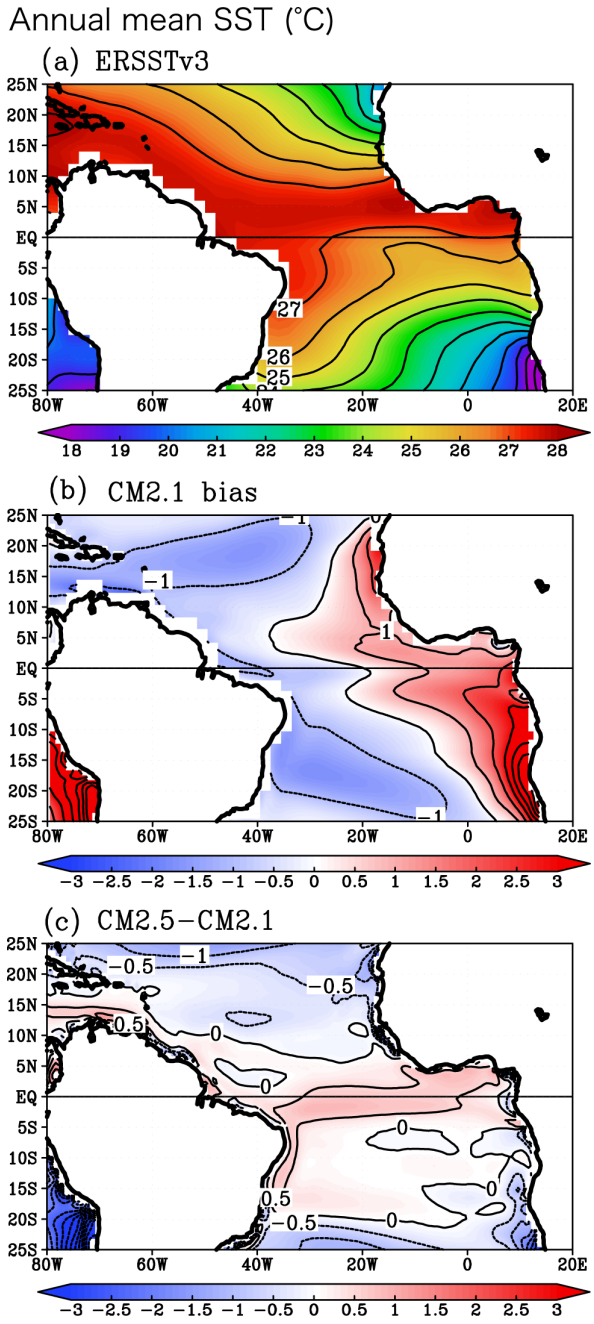

2

3 Fig. 1: (a) Annual mean SST from the ERSSTv3 data (°C). The contour interval is 1°C.
4 (b) Annual mean SST bias in CM2.1 from the ERSSTv3 data. The contour interval is
5 1°C. (c) Difference in annual mean SST between CM2.5 and CM2.1. The contour
6 interval is 0.5°C. Note that the SST bias in CM2.1 and CM2.5 is almost same, if the
7 HadISST dataset is used as a reference.

Fig.2

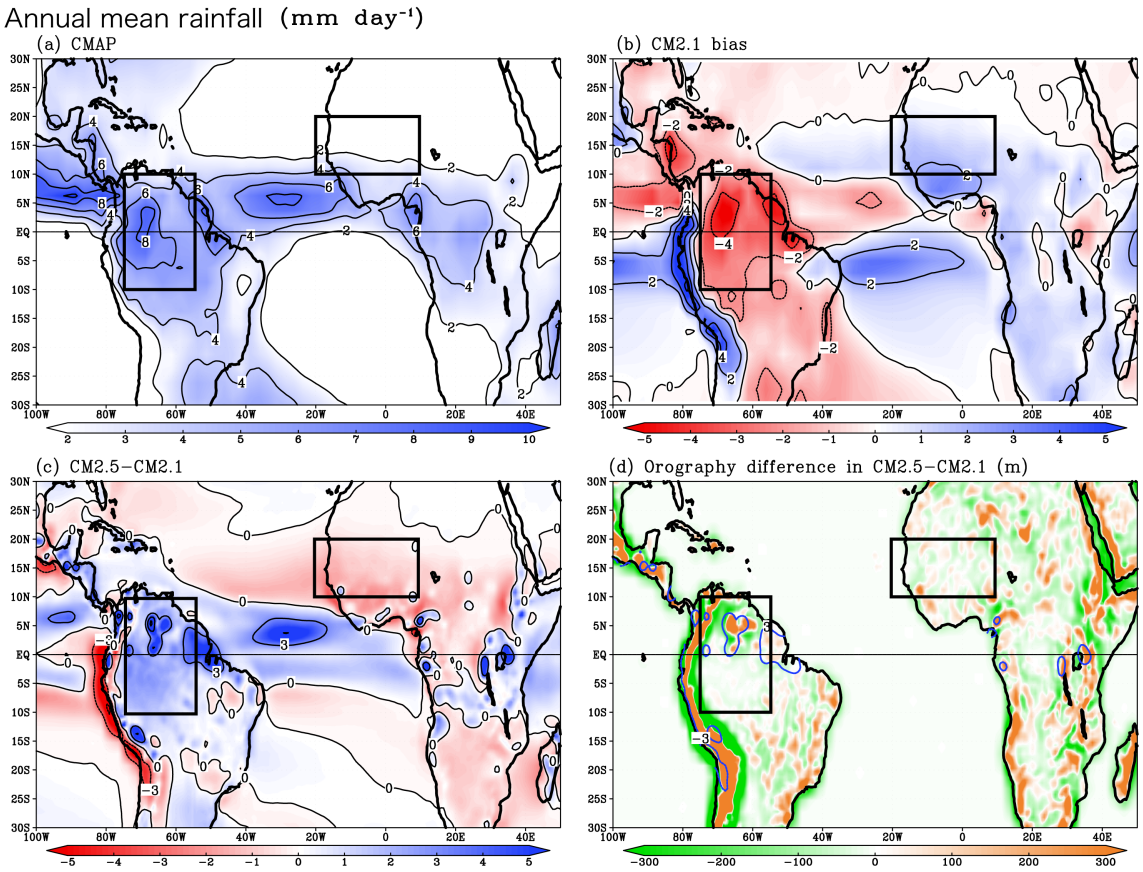

Fig. 2: (a) Annual mean rainfall from the CMAP data (mm day^{-1}). The contours interval is 2 mm day^{-1}. (b) Annual mean rainfall bias in CM2.1 from the CMAP data (mm day^{-1}). The contour interval is 2 mm day^{-1}. (c) Difference in annual mean rainfall between CM2.5 and CM2.1. The contours interval is 3 mm day^{-1}. (d) Difference in orography between CM2.5 and CM2.1 (m). The blue contour shows difference in annual mean rainfall between CM2.5 and CM2.1, same as (c). The Sahel region (20°W-10°E, 10°-20°N) and the northern South American region (75°-55°W, 10°S-10°N) are shown by solid boxes.

Fig.3

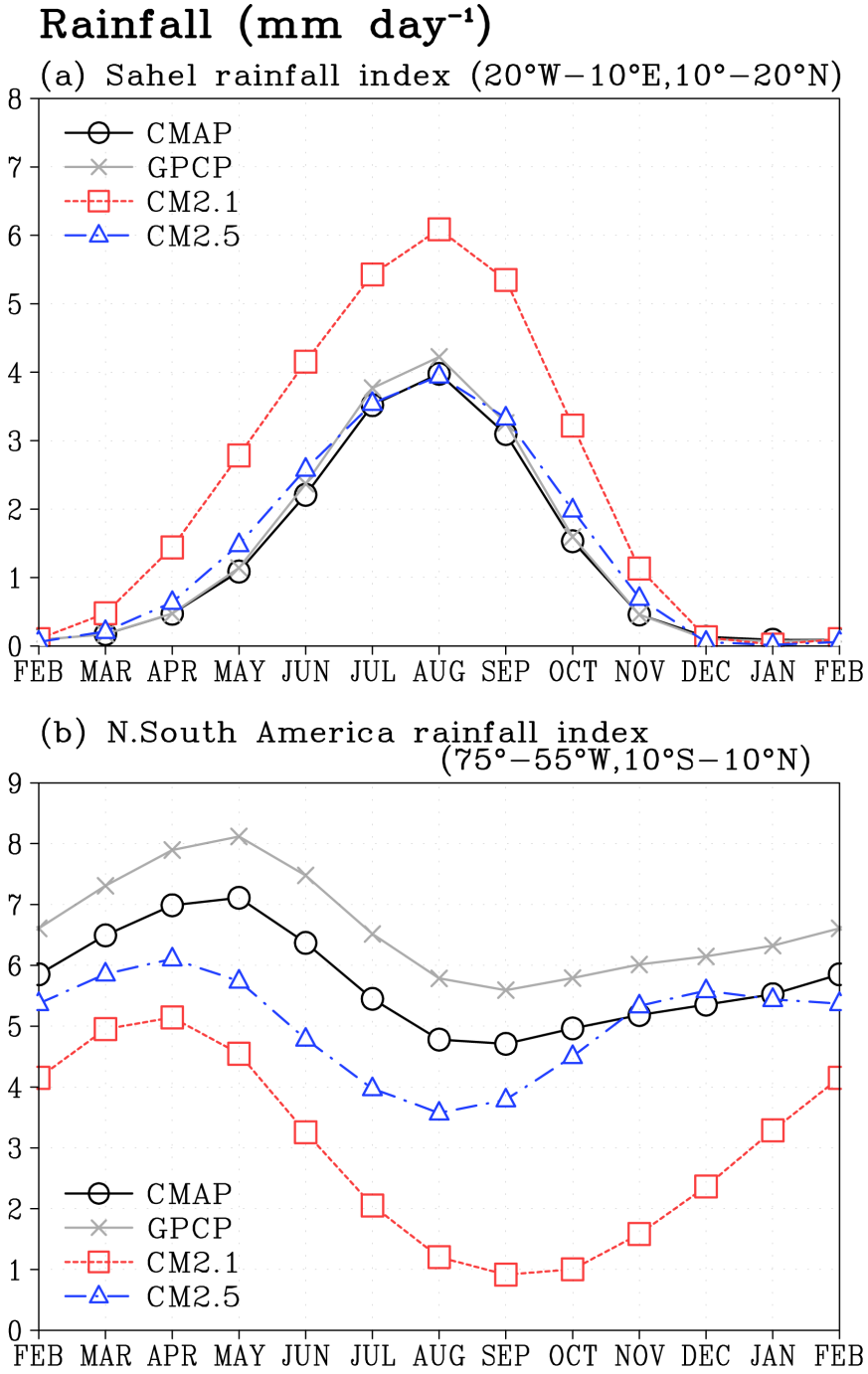

Fig. 3: (a) Seasonal cycle of rainfall averaged in the Sahel region (20°W-10°E, 10°-20°N) (mm day^{-1}). This index is also used in Lu and Delworth (2005). (b) Same as (a), but for the northern South American region: 75°-55°W, 10°S-10°N.

Fig.4

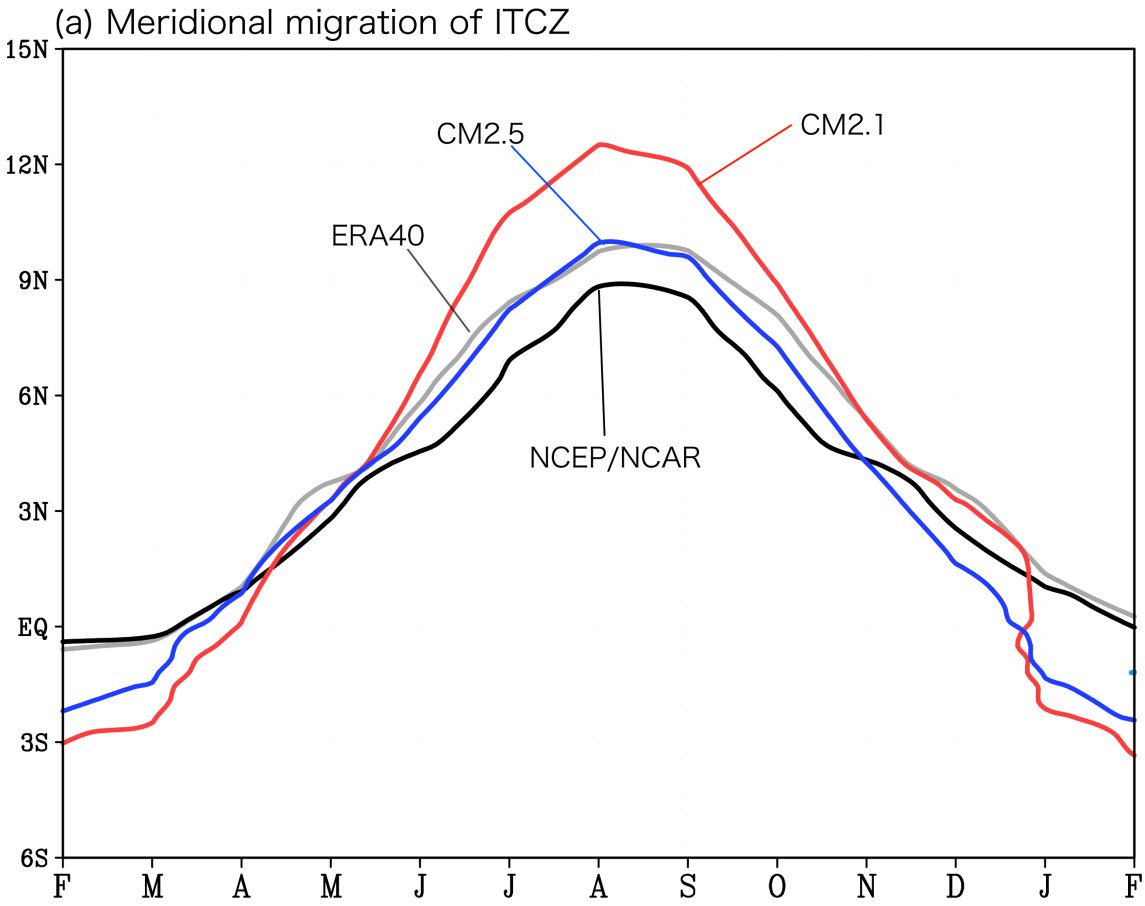

Fig. 4: (a) Seasonal meridional migration of the Atlantic ITCZ, which is defined as zero meridional wind stress averaged in 50°-20°W.

1 Fig.5

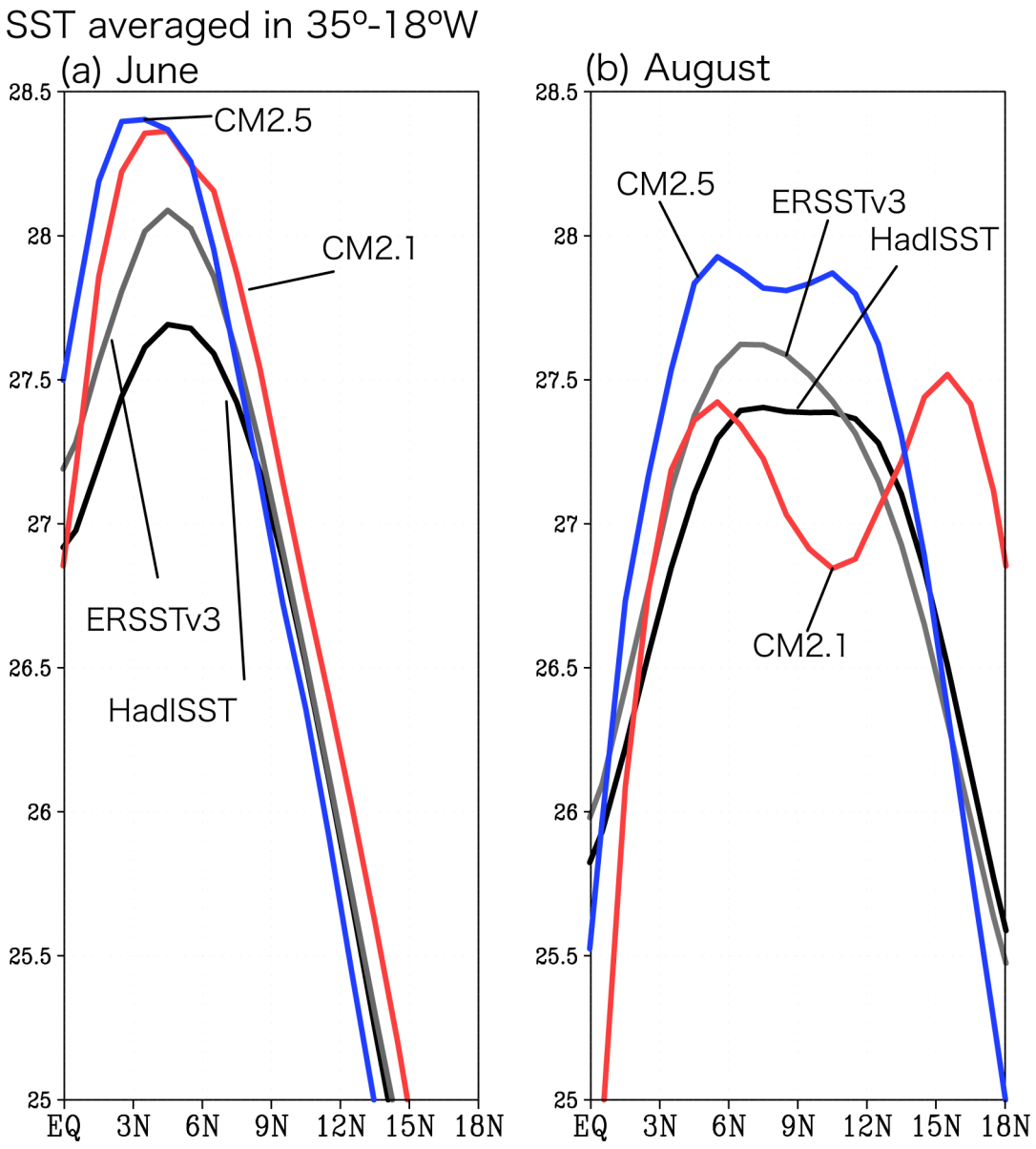

2

3 Fig. 5: Climatological SST averaged in the northeastern tropical Atlantic (35°-18°W)

4 in (a) June and (b) August.

Fig.6

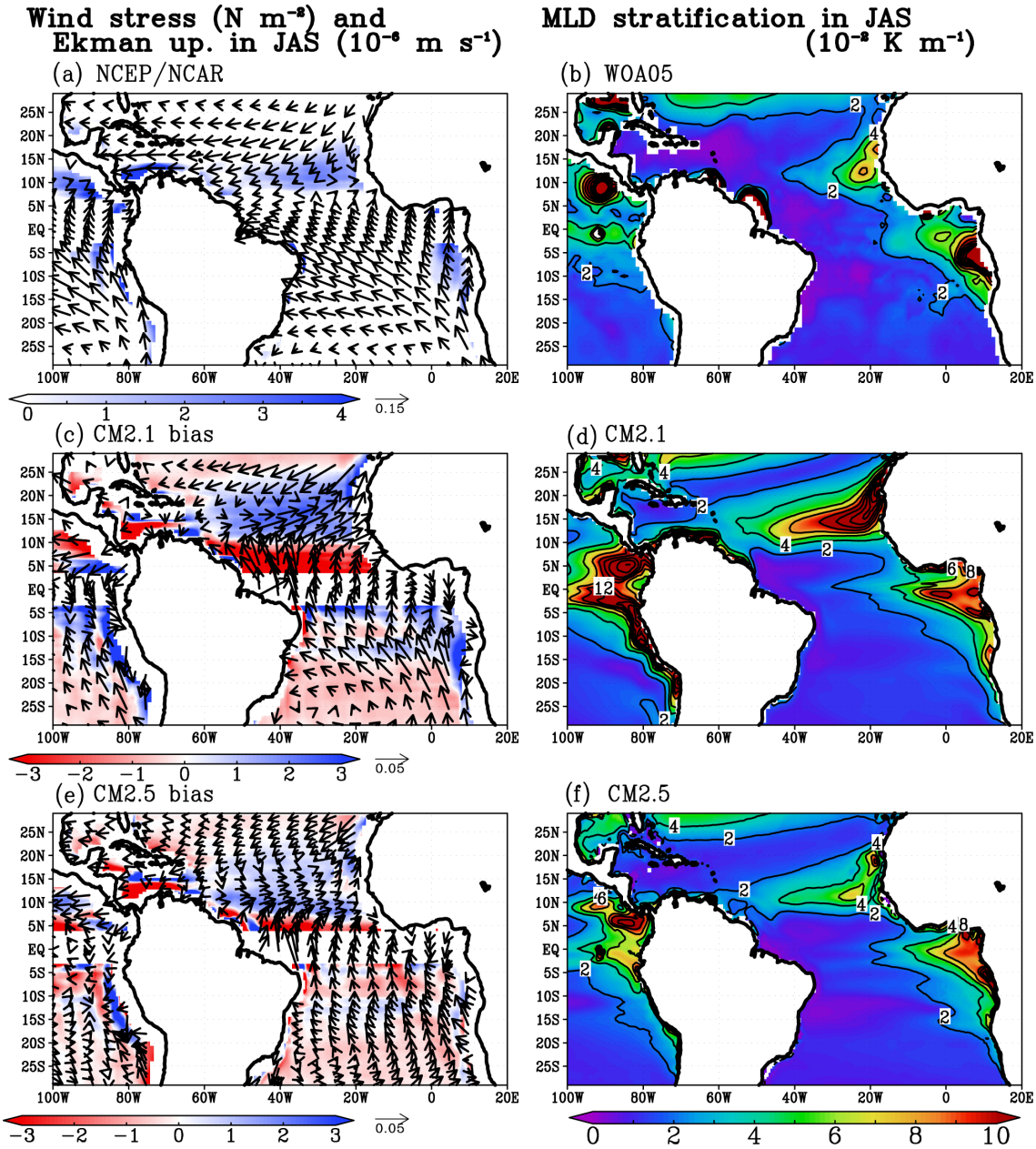

Fig. 6: (a) Climatology of wind stress (N m^{-2}; vector) and Ekman upwelling (shaded; 10^{-6} m s^{-1}) in July-September from the NCEP/NCAR reanalysis data. Upwelling is shown by blue shading, while downwelling is shown by red shading. (b) Climatology of stratification around mixed-layer depth, $\frac{T_{mix}-T_e}{H_{mix}}$, averaged in July-September from the WOA05 data (10^{-2} K m^{-1}), (d) CM2.1 and (f) CM2.5. The contour interval is 0.2× 10^{-2}K m^{-1}. (c) Same as (a), but for CM2.1 bias and (e) CM2.5 bias from the NCEP/NCAR reanalysis data.

Fig. 7

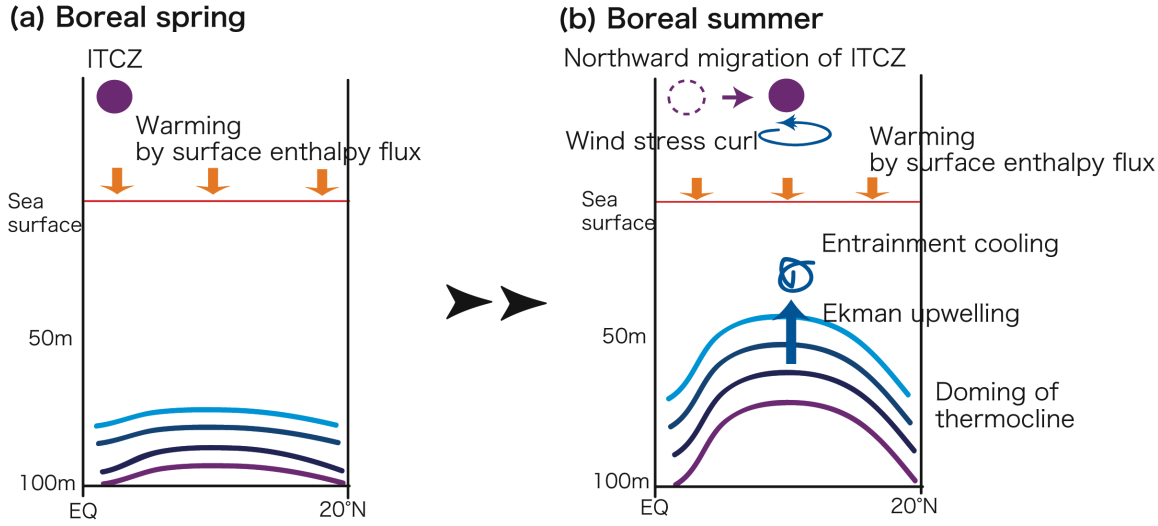

Fig. 7: Schematic diagram of the seasonal variations in the northern tropical Atlantic. (a) In boreal spring, surface enthalpy flux warms the SST and the mixed-layer depth is deep. (b) In boreal summer, the Guinea Dome develops through the Ekman upwelling associated with the northward migration of the ITCZ. The Guinea Dome cools the mixed-layer temperature through entrainment as a counteracting role of warming tendency by surface enthalpy flux.

Fig.8

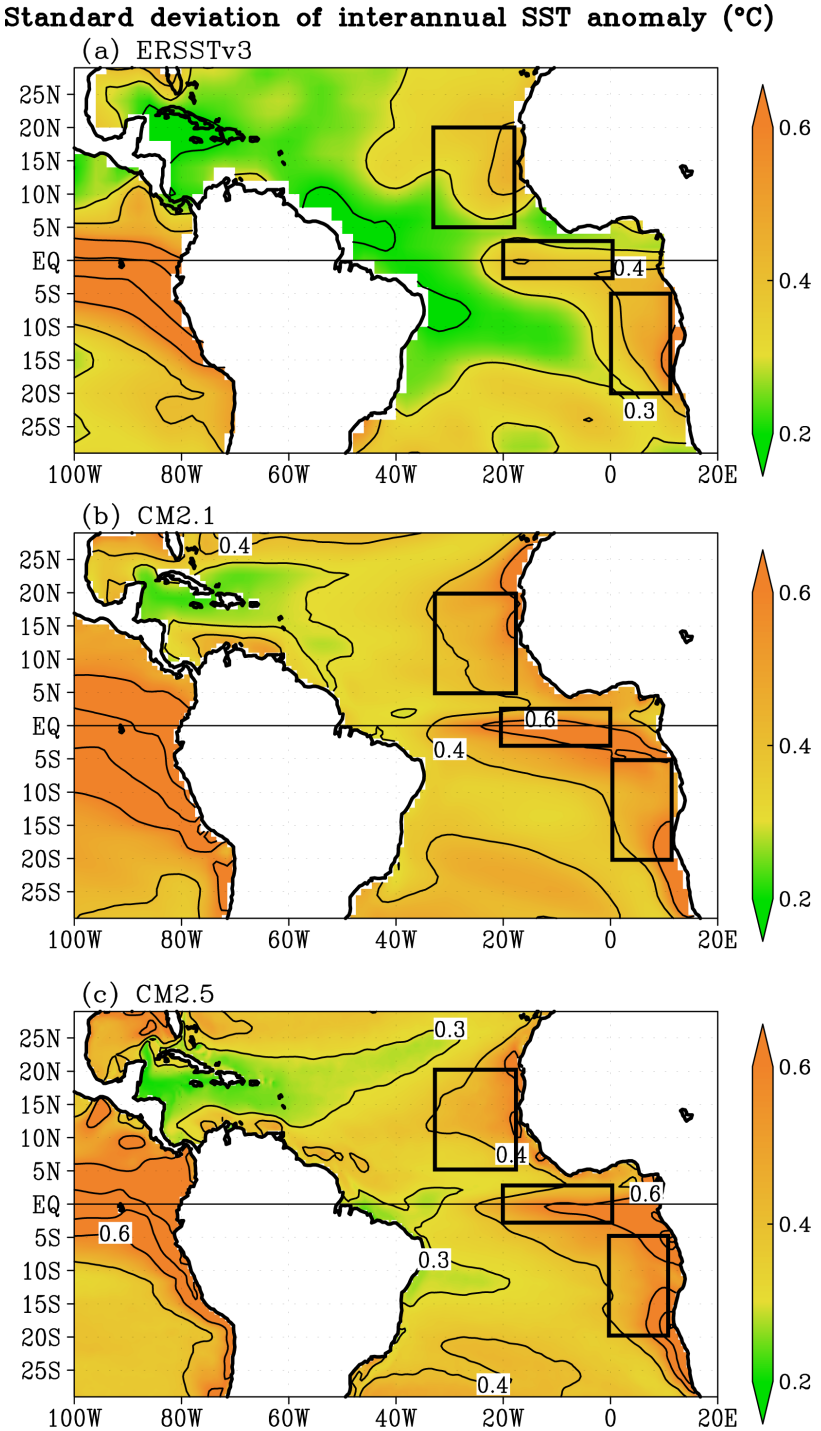

Fig. 8: (a) Horizontal map of the standard deviation of the interannual SST anomaly averaged in whole season from the ERSSTv3 data, (b) CM2.1, and (c) CM2.5 (°C). Contour shows 0.2, 0.3, 0.4, 0.6, 0.9, and 0.13°C. The northern tropical Atlantic region (NTA: 35°-18°W, 5°-20°N), the Atlantic Niño index (ATL3: 20°W-0°, 3°S-3°N), and the Angola-Benguela area (ABA: 0°-20°E, 25°-5°S) are shown in boxes.

Fig.9

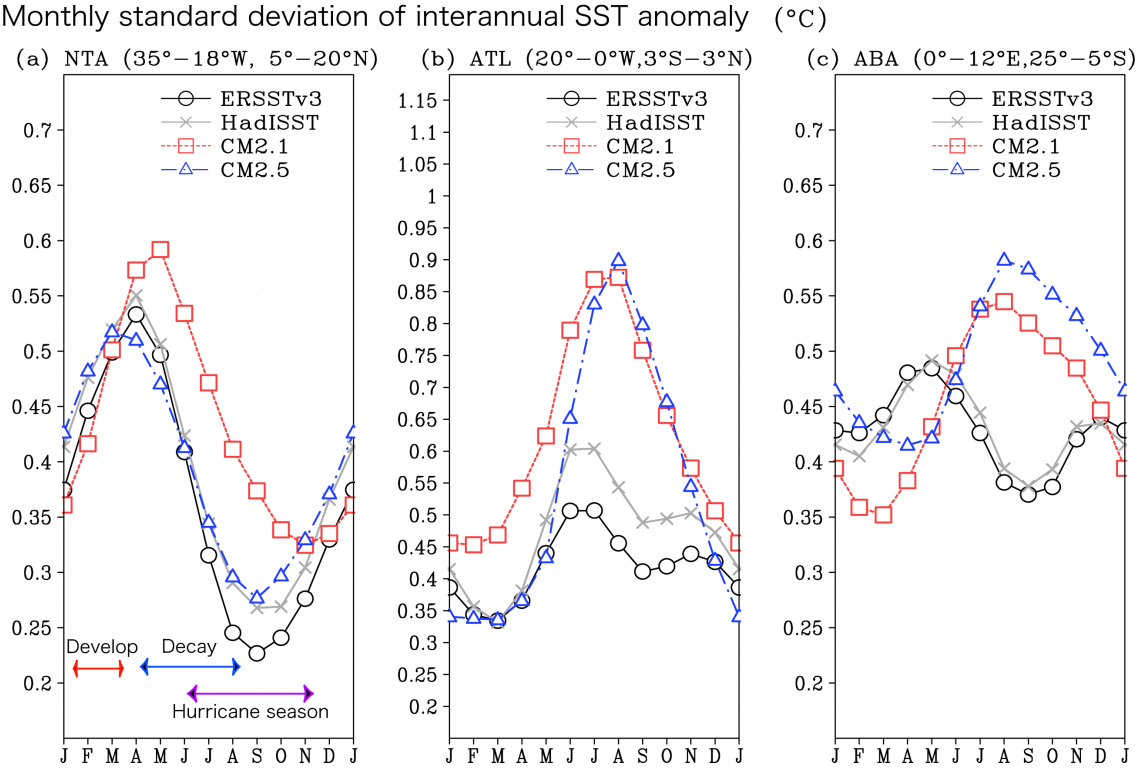

Fig. 9: (a) Monthly standard deviation of the interannual anomaly of SST from ERSSTv3 (bar), HadISST (grey line), GFDL-CM2.1 (red line), and CM2.5 (blue line) averaged in the northern tropical Atlantic region (NTA: 35°-20°W, 5°-20°N), (b) the Atlantic Niño index (ATL3: 20°W-0°, 3°S-3°N), (c) the Angola-Benguela region (ABA: 0°-20°E, 25°-5°S). We note that vertical scale in (b) is different from that in (a) and (c).

Fig.10

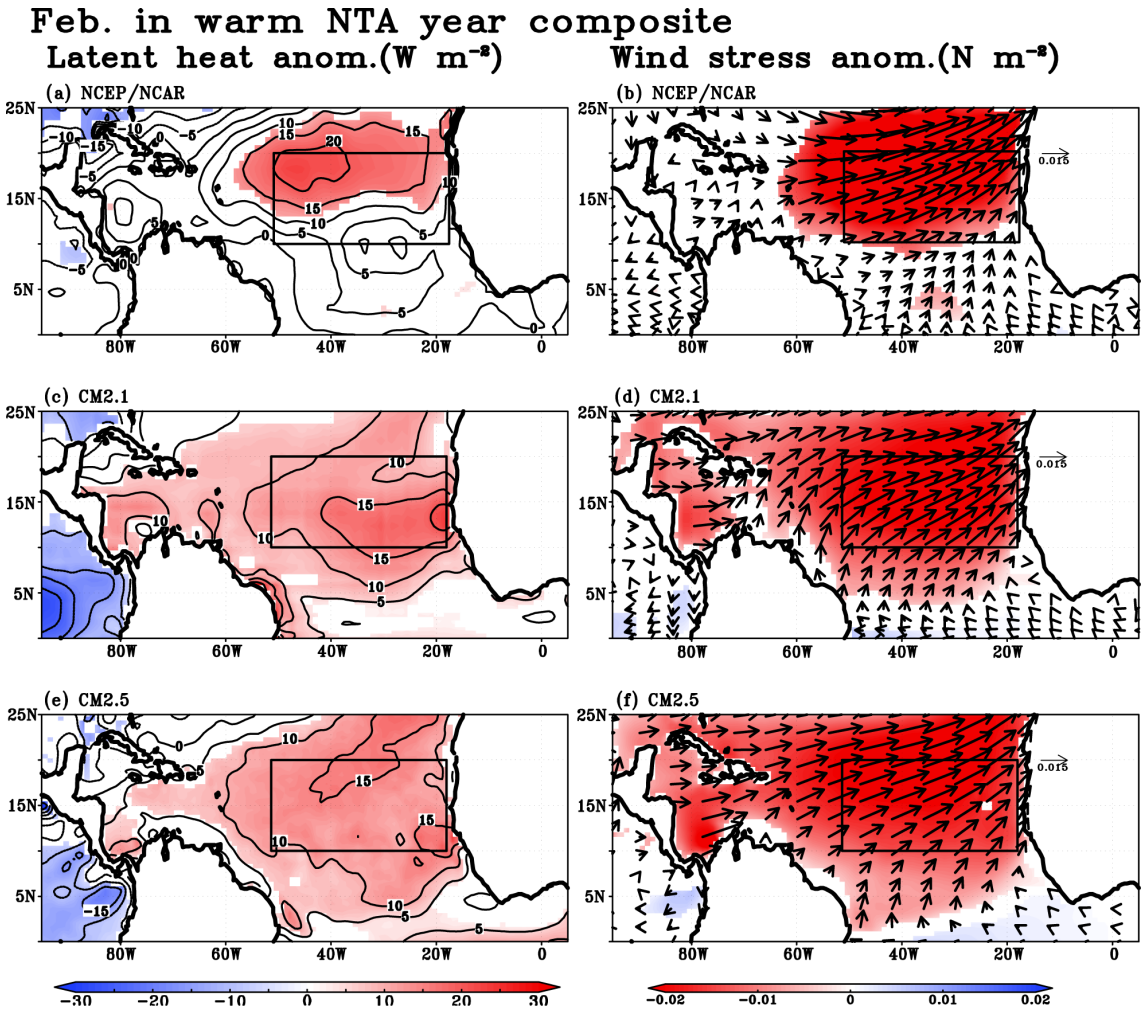

Fig. 10: (a) Composite anomalies for the latent heat flux from NCEP/NCAR reanalysis data in February of the warm NTA years (W m^{-2}). Positive values shows warming ocean. Contour interval is 5W m^{-2}. Color shading denotes anomalies above 90% significance level. (b) Same as (a), but for wind stress (N m^{-2}; vector). Red (blue) shading denotes negative (positive) wind stress anomalies above 90% significance. (c) Same as (a), but for CM2.1 and (e) CM2.5. Color shading denotes anomalies above 99% significance level. (d) Same as (b), but for CM2.1 and (f) CM2.5. Red (blue) shading denotes weak (strong) anomalies above 99% significance.

Fig. 11

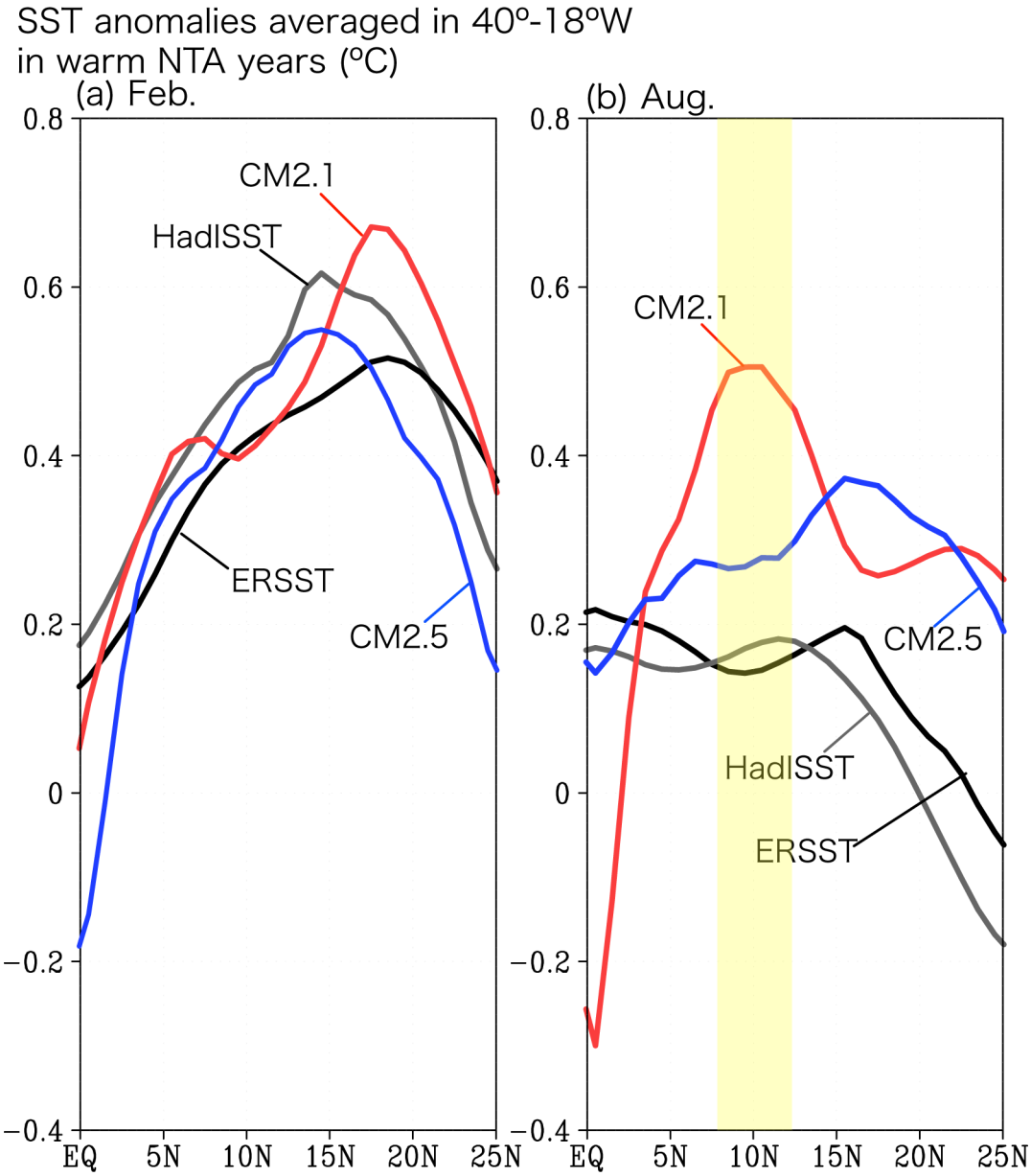

Fig.11: Composite anomalies for SST averaged in 40°-18°W in (a) February and (b) August of warm NTA years (°C). The maximum bias in SST between observations and CM2.1 appears in 8°-12°N during August.

1 Fig. 12

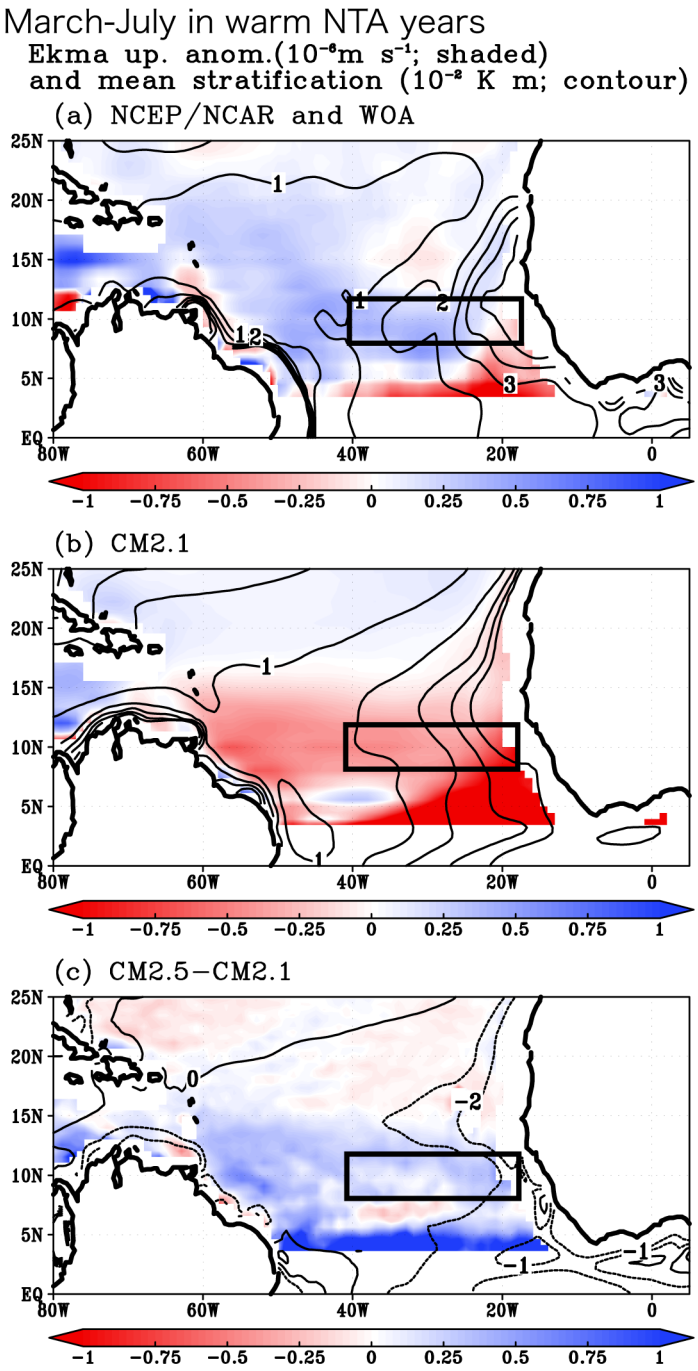

2

3 Fig.12: (a) Composite anomalies for Ekman upwelling in March-July of warm NTA
4 SST years from NCEP/NCAR reanalysis data (shaded; 10^{-6}m s^{-1}). Red (blue) shading
5 denotes downwelling (upwelling) anomalies. Contour shows climatology of
6 stratification around mixed-layer depth, $\frac{T_{mix} - T_e}{H_{mix}}$, in March-July from WOA05 data

1 (10^{-2}K m^{-1}). Contour interval is 1×10^{-2}K m^{-1}. (b) Same as (a), but for CM2.1. (c) Same
2 as (a) but for the differences between CM2.5 and CM2.1.

1 Fig. 13

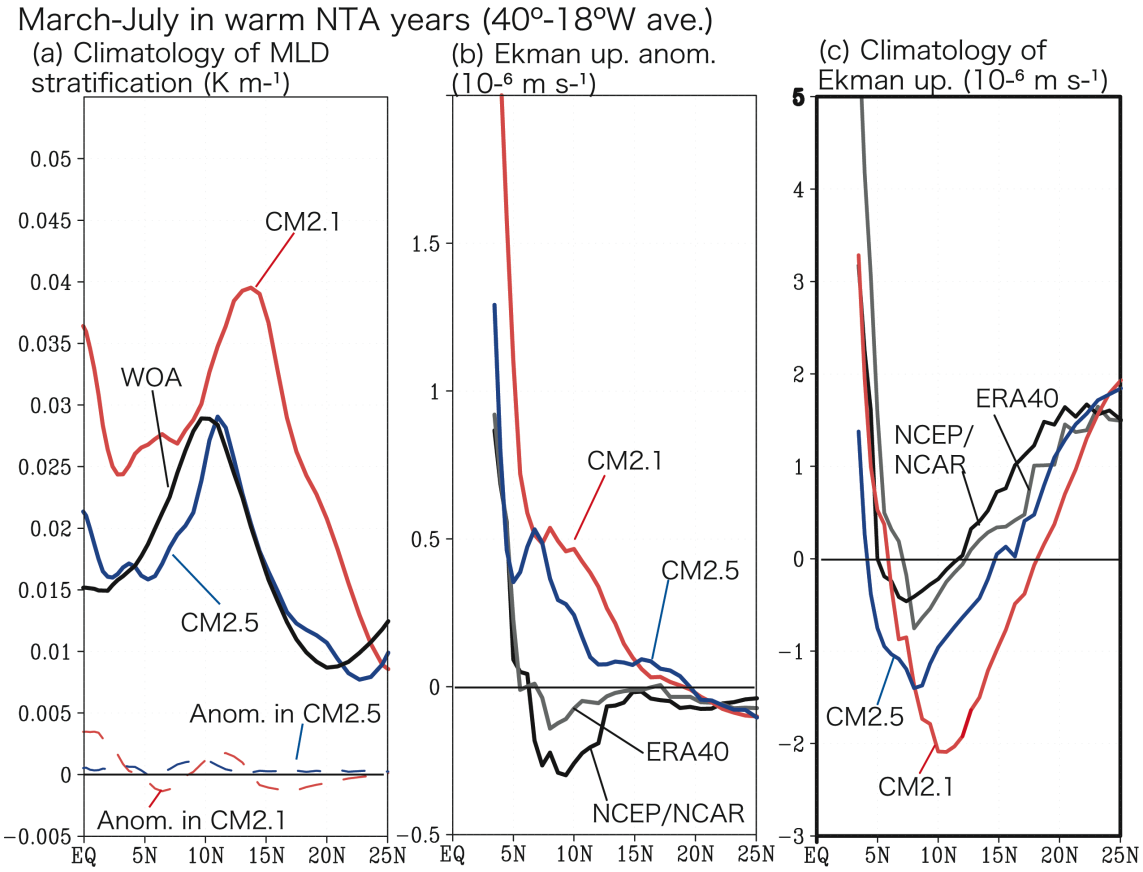

2

3 Fig. 13: (a) Climatology of ocean stratification around mixed-layer depth, $\frac{T_{mix}-T_e}{H_{mix}}$,

4 averaged in 40º-18ºW during March-July (thick lines; K m^{-2}). Note that interannual

5 anomalies in models are less than 5% of the mean values (dashed lines). (b) Composite

6 anomalies for Ekman upwelling in 40º-18ºW during March-July in warm NTA years

7 (10^{-6} m s^{-1}). Positive (Negative) values show downwelling (upwelling) anomalies. (c)

8 Climatology of Ekman upwelling averaged in 40º-18ºW during March-July (10^{-6} m s^{-1}).

9 Positive (Negative) values show downwelling (upwelling).

Fig.14

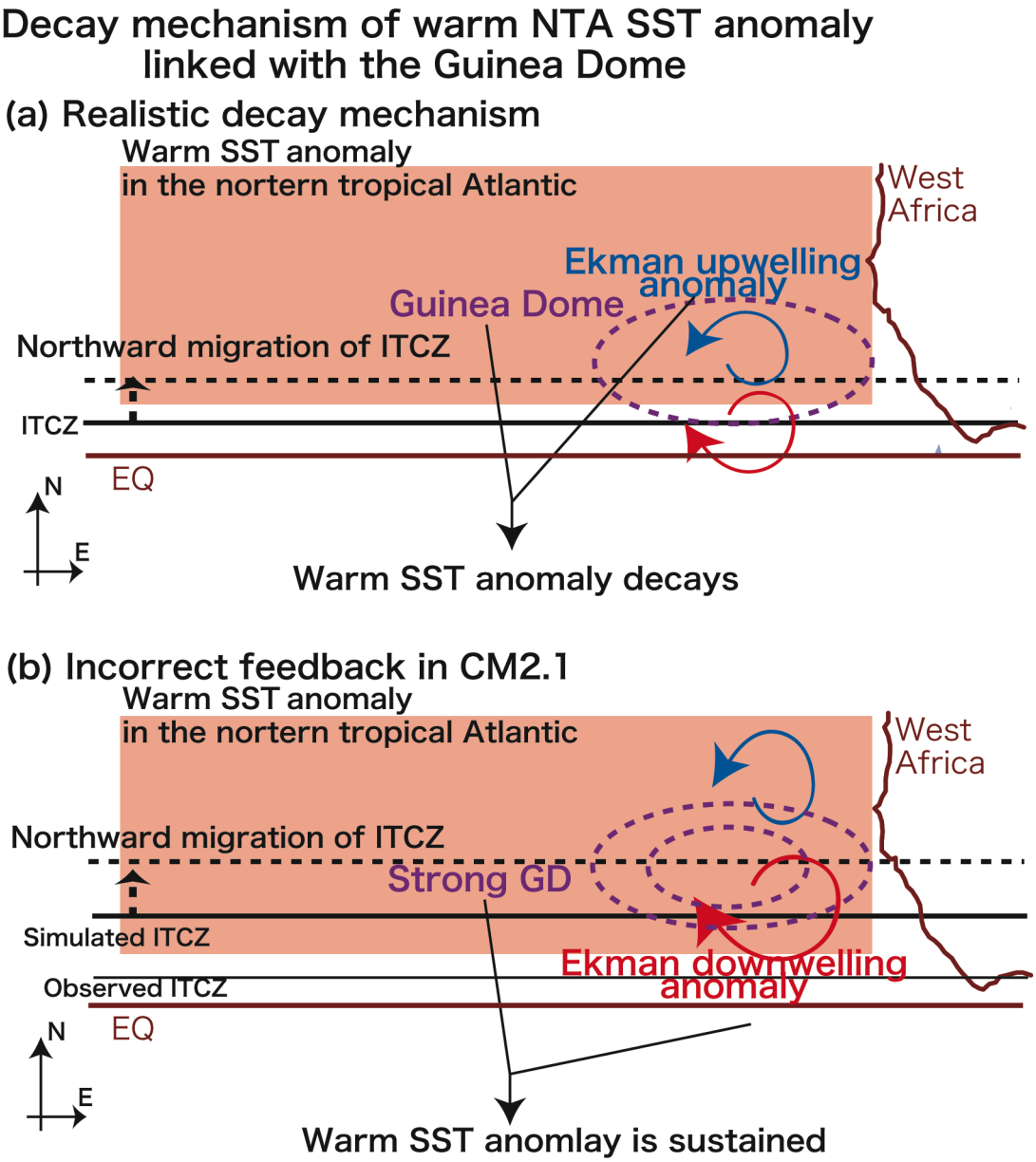

Fig.14: Schematic diagram for (a) the boreal summer decay mechanism of the warm SST in the northern tropical Atlantic linked with the Guinea Dome suggested by observational estimate and Doi et al. (2010). (b) The incorrect role of the Guinea Dome is found in CM2.1.